CHALMERS

Multidisciplinary Conceptual Design of a Transonic High Pressure Compressor

Master's Thesis in the Fluid Mechanics

FUNDA ERSAVAS

Department of Applied Mechanics
Division of Fluid Mechanics
CHALMERS UNIVERSITY OF TECHNOLOGY
Göteborg, Sweden 2011
Master's Thesis 2011:56

MASTER'S THESIS 2011:56

Multidisciplinary Conceptual Design of a Transonic High Pressure

Master's Thesis in the Fluid Mechanics

FUNDA ERSAVAS

Department of Applied Mechanics
Master's Thesis in the Fluid Mechanics
CHALMERS UNIVERSITY OF TECHNOLOGY
Göteborg, Sweden 2011

Multidisciplinary conceptual design of a transonic high pressure compressor

Master's Thesis in the Fluid Mechanics

FUNDA ERSAVAS

© FUNDA ERSAVAS, 2011

Master's Thesis 2011:56
ISSN 1652-8557
Department of Applied Mechanics
Division of Fluid Mechanics
Chalmers University of Technology
SE-412 96 Göteborg
Sweden
Telephone: + 46 (0)31-772 1000

Chalmers Reproservice / Department of Applied Mechanics
Göteborg, Sweden 2011

Multidisciplinary conceptual design of a transonic high pressure compressor

Master's Thesis
Department of Applied Mechanics
Division of Fluid Mechanics
Chalmers University of Technology

ABSTRACT

The aim of this work is to develop a systematic approach for multidisciplinary high pressure transonic axial compressor conceptual design. Several aspects have to be taken into account when establishing a new compressor design. Apart from developing a successful aerodynamic design that provides high efficiency and maintaining a design that allows manufacturing at a reasonable cost, structural dynamics and rotor dynamic considerations have to be taken to ensure a mechanically stable operation. It is quite common that a seemingly well designed compressor exhibits rotor dynamic instability at some rotational speed and that this requires re-designing the machine.

This report presents the initial results of a multidisciplinary conceptual design of a five stage transonic high pressure compressor that has an overall pressure ratio of 4.46, an inlet temperature of 401.4K an inlet pressure of 132.9 kPa and a mass flow of 14.18 kg/s. Basic parameters such as blade masses, disc stress calculations and conceptual disc design were carried out using existing tools and analytical techniques. The work consists of setting up a basic Finite Element (FE) model using the ANSYS software and subsequently a basic rotor dynamic model in the DyRoBeS tool. In order to evaluate these parameters, basic aerodynamic theory of the axial flow compressor was used.

The work starts with a brief introduction to the fundamentals of gas turbine theory and results in a basic aerodynamics design. The aerodynamic theory of axial flow compressors is used to calculate design parameters such as temperatures and pressures for all stages, geometrical parameters, velocity triangles, etc. After the aerodynamic calculation, weight and stress calculation for the compressor disks follows. Since weight is one of the most important parameters when designing a gas turbine engine, an accurate weight estimation method is desired. In the beginning of the design process, several different approaches can be used in order to achieve the same functionality. In this report, an approach similar to the weight estimation method WATE (Weight Analysis of Turbine Engines) was used to calculate rotor and stator blade weights. Subsequent steps are comprised of modelling the disks. A preliminary design calculation is carried out in such a way that the whole disk is approximated as a superposition of several coupled elementary parts: a ring disc, a section with hyperbolic shape and a section with a linearly varying thickness. This basic non-linear analytic procedure is followed by creating the basic FE model using the ANSYS software to determine best shape of the bladed disc (blisc) and vibrational characteristics of the blisc geometries. After this step, a basic rotor dynamic model in the DyRoBeS tool is established to correctly continue the analysis and to learn the behaviour of the compressor during operation at high speed.

Key words: Transonic compressor, conceptual aerodynamic design, gas turbine rotor dynamic analysis

Contents

1 Introduction

This work has been carried out as a part of a joint project between Volvo Aero and Chalmers University of Technology. The project aim is to develop methods that can design and analyze engine concepts that will be introduced around year 2025. In line with this purpose, this project has several parts as the performance of compressors, combustors, turbines, and conceptual whole engine design. The objective of this master thesis is to perform an initial design study of a transonic high pressure compressor for an open rotor aero engine. The study includes preliminary aerodynamic design and mechanical design in order to provide high efficiency and mechanically stable operation. The work puts special emphasis on rotor dynamic and structural mechanics.

Calculated results consist of mechanical data as well as aerodynamic performance parameters. The output will allow the user to obtain sufficient input parameters for a preliminary aerodynamic and rotor dynamic analysis as well as an insight into the engine structure.

1.1 Compressor Design Procedure

A schematic diagram representing the most general design procedure is shown in Figure 1.1. This diagram shows the interrelationship between different disciplines, such as thermodynamics, aerodynamics, and mechanical design and emphasizes the need for feedback between various specialists. All these stages must consider manufacturing feasibility. During the multistage design the most important thing is flow of information between different sections. Every designer who is not important which department must be careful in that all sections affect each other. The area where is inside the dashed line imagines application field of this master thesis.

The design process of a new engine starts from market research and customer requirements. Both of these create specifications that eventually lead to component specifications. The definitions of component requirements are rarely a simple statement of required power and efficiency. Other factors of major importance which vary with the application include component weight, cost, volume, life, and many of these criteria act in opposition.

The first main step in the design process is the thermodynamic design. This is already a detailed calculation taking a number of important factors, such as excepted component efficiencies, air–bleeds, variable fluid properties and pressure loses into account. This analysis is carried out over a range of pressure ratios and turbine inlet temperatures.

After the thermodynamic design point and off-design point calculations have determined the airflow, pressure ratio and turbine inlet temperature, attention can be turned to the aerodynamics design of the turbomachinery. It is now possible to determine annulus dimensions, rotational speeds and numbers of stages. The aerodynamic design of the turbo machinery must take into account manufacturing feasibility from the outset.

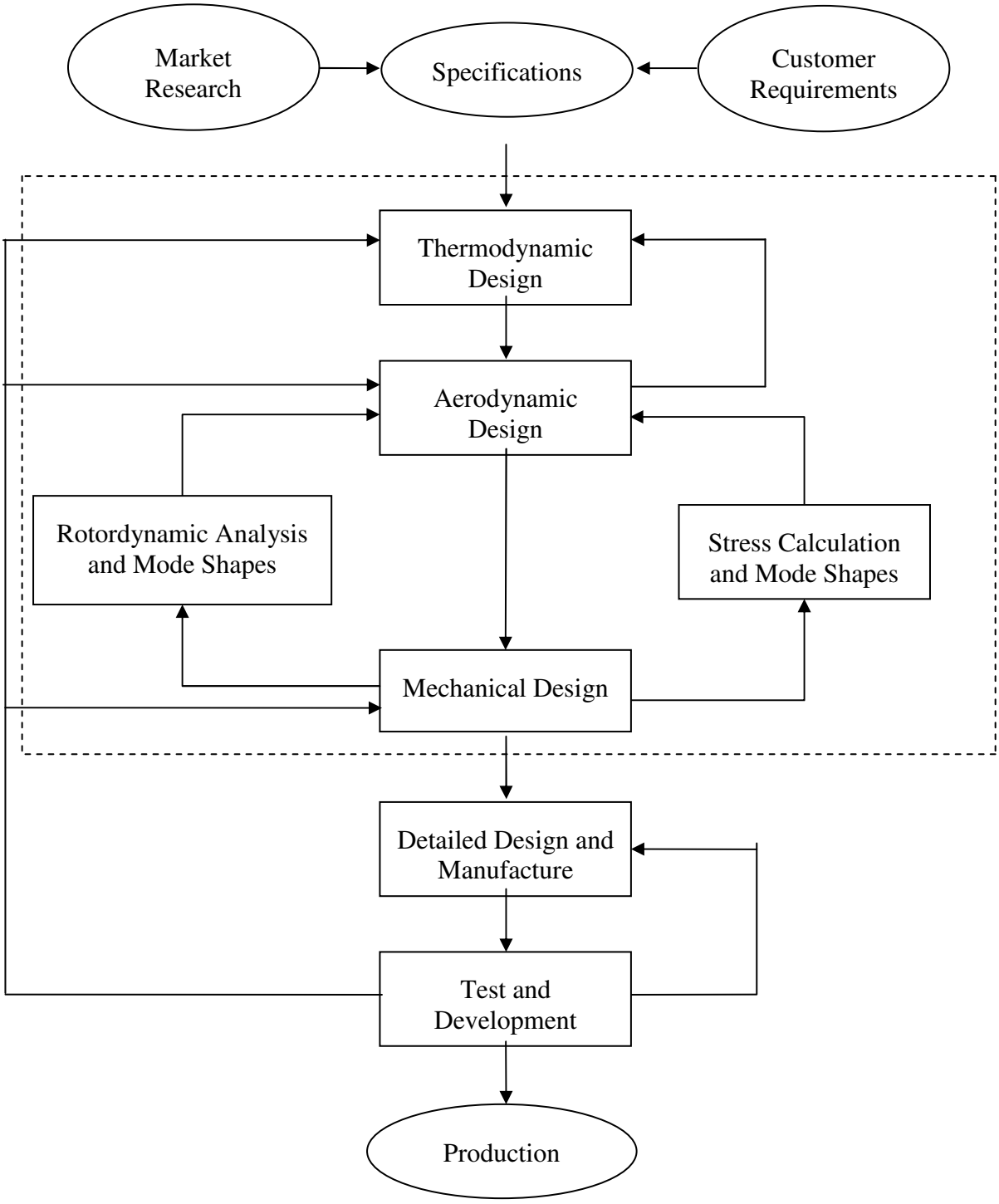

Figure 1.1 Schematic diagram of design procedure

The mechanical design can start only after the thermodynamic and aerodynamic design teams have established the key dimensions of the engine. It will then probably be found that stress and vibrations problems may lead to further changes, the

requirements of the stress and aerodynamics groups often being in opposition. At the same time as these studies are proceeding, off-design performance and control system design must be considered.

Rotordynamic analysis is based on the whole gas generator vibration because rotors in compressor are only one part of a dynamic system; also there are turbines, bearings and their supports in the dynamic system. In order to take high efficient performance from the engine, high rotational speeds is necessary and eventually effects of asymmetry, imbalance and misalignments between components create dynamic loads on the engine. Furthermore, the design of the engine must be carried out with considerations for future growth.

1.2 Axial Compressors

A compressor is a machine used for increasing the pressure of a working fluid. Compressors can be classified as positive–displacement or dynamic type. Nowadays dynamic type compressors, such as centrifugal and axial flow compressors, are used for aeronautics. Predominantly the working fluid is air. This study focuses on an axial flow compressor; the most common design choice when there is a requirement for a high flow rate.

During the Second World War, the development of gas turbines made very rapid progress at especially simple turbojet units. On the one hand German efforts were based on the axial flow compressor while on the other hand British developments used the centrifugal compressor. Before long, British developments recognized that axial flow compressors were more suitable for large engines because axial flow compressor had the potential not only for higher pressure ratio but also higher efficiency than the centrifugal compressor. Another major advantage was the larger flow rate possible for a given frontal area. This potential gain has now been fully realized as the result of intensive research into the aerodynamics of axial compressors: the axial flow machine dominates the field for large powers and the centrifugal compressor is restricted to the lower end of the power spectrum where the flow is too small to handle efficiently by axial blading. Early on, overall compressor pressure ratios was around 5:1 and required around 10 stages but nowadays turbofan engines have pressure ratio exceeding 40:1 (Saravanamutto, 2009).

The design of compressors is one of the major fluid mechanics problems in the field of turbomachinery. The flow is always subjected to an adverse pressure gradients, and the higher the pressure ratio, the more difficult the design of the compressor becomes. Some advantages of axial compressors are, as already mentioned, high efficiency, high speed capability, higher flow for given size and continuity flow. Disadvantages are low pressure ratio per stage, narrow flow range, fragile and expensive blading.

1.3 Components of the Gas Generator

Every gas turbine engine has a compressor, combustion chamber and turbine. These components are called the core of the engine. The core is also referred to as the gas generator. The layout is shown diagrammatically in Figure 1.2. This chapter is concerned with the main components of gas the generator.

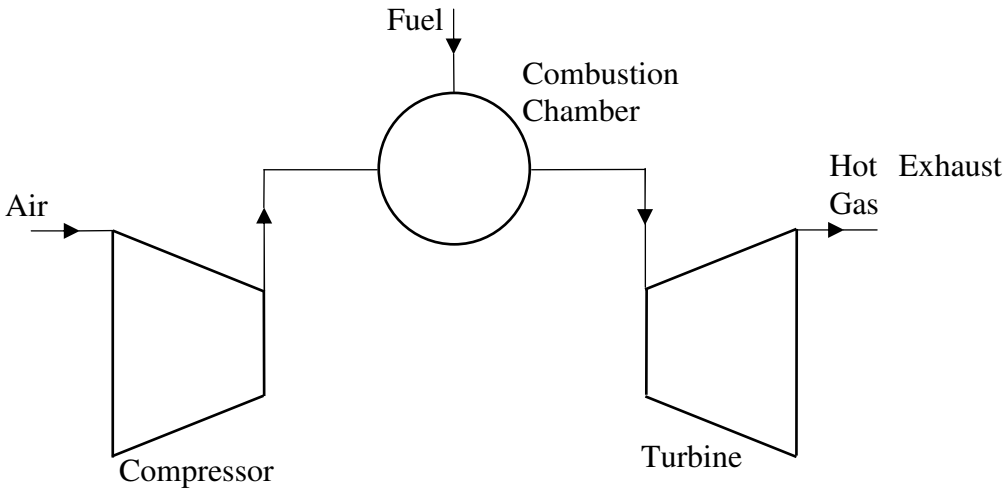

Figure 1.2 A simple gas generator

The Axial Compressor

The first stage of the gas generator is the compressor which increases the pressure of the incoming air before the air enters the burner. The compressor performance influences to a large degree the total engine performance. In the axial compressor, the air flow is parallel to the axis of rotation.

The axial compressor consists of a series of stages. Each stage comprises a row of rotor blades followed by a row of stator blades. They are the main components of the compressor. Rotors are connected to the central shaft and rotate at high speed and stators are fixed parts. The working fluid is initially accelerated by a row of rotating airfoils (rotor blades), and then decelerated in the row of stationary blades (stator blade) passage. During this process kinetic energy transferred in the rotor is converted to static pressure. After every stage the pressure is increased within possible aerodynamic limits. This process is repeated in as many stages as are necessary to yield the required overall pressure ratio. Compressors and turbines are connected through a shaft rotating at a given rotational speed.

The Combustion Chamber

The combustion chamber, or burner, is the second component in the engine core where air is mixed with a relatively small amount of fuel and then ignited. Inside the combustion chamber there are several nozzles to spray fuel into the flow. The fuel burns with oxygen in the compressed air. This burned gas has a high temperature and energy level.

The Turbine

After the burner, high energy high density airflow is entering the turbine. As the airflow passes through the turbine, the turbine blades rotate and hence the shaft also rotates. This rotation takes some energy from the burned high energy airflow to drive the compressor. The remaining energy is used to fulfil the engine thrust requirement.

2 Fundamental Theory

The overall gas turbine design process is shown in Figure 1.1 and the mechanical design is clearly one of the critical areas. The mechanical design process cannot be started before an initial aerodynamic and thermodynamic design has been completed. Preliminary thermodynamic analysis determines mass flow, pressure ratio, and the temperature distribution through the gas path. The aerodynamic design then uses these results to determine the number of stages of the compressors and turbines, the shaft rotational speed and ultimately the geometry of the compressors and turbines. In this chapter general elementary theory of thermodynamic, aerodynamic and mechanical design concepts is explained.

2.1 Thermodynamic and Aerodynamic Design

2.1.1 T–s Diagram

Figure 2.1 shows a sketch of a temperature enthalpy diagram of a typical compressor stage but only if the flow is steady and the system is adiabatic. The diagram also shows the effect of losses in both the rotor and the stator within a stage. As mentioned before all power is absorbed in the rotor, and the stator transforms the kinetic energy to increase the static pressure. This is why the stagnation temperature remains constant. The stagnation pressure is only increased within the rotor. Within the stator there is a small decrease because of fluid friction (Saravanamutto, 2009).

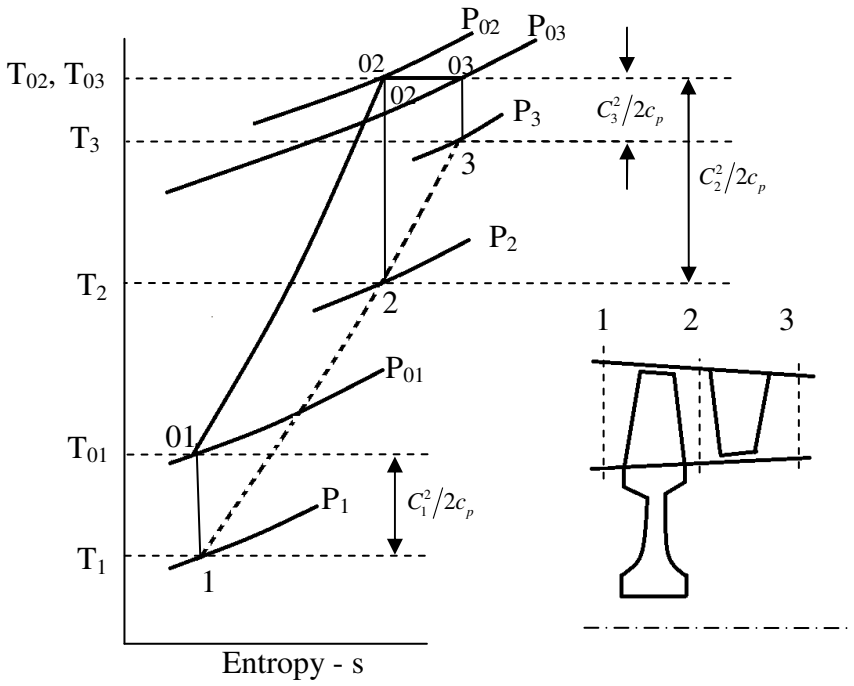

Figure 2.1 T – s diagram and compressor stage

2.1.2 Velocity Triangles

The density of the working fluid changes at every stage. Also, annulus area and some geometric characteristics changes as well. Simple thermodynamic and aerodynamic methods show can be used to model how they are changing but not to determine blade shapes and variation of rotor inlet/outlet, stator inlet/outlet velocities with changing axial velocity and radii (Wilson, 1998). The velocity triangle is the most fundamental process to get clear picture, how a compressor blade row is operating and to relate flow properties and blade design parameters. The velocity triangle is generally described at the mean height of the blade where the peripheral velocity is U and it assumes that the flow occurs on a cylindrical surface. Figure 3 shows the velocity triangle and velocity vectors for a typical stage.

The velocity components of the working fluid can be expressed in two velocity vectors, the absolute and the relative velocity. The fluid enters the rotor with an absolute velocity, C_1, and has an angle, α_1, from the axial direction. Combining the absolute velocity with the blade speed, U, gives the relative velocity, V_1, with its angle β_1. The mechanical energy from the rotors will be transferred to the working fluid.

This energy absorption will increase the absolute velocity of the fluid. After leaving the rotor the fluid will have a relative velocity, V_2, with an angle, β_2, determined by the blade outlet angle. The fluid leaving the rotor is consequently the air entering the stator where a similar change in velocity will occur. Here the relative velocity, V_2, will be diffused and leaving the stator with a velocity, C_3, at an angle, α_3. Typically the velocity leaving the stator will be the same as the velocity entering the rotor in the next row, $C_3 = C_1$, and $\alpha_3 = \alpha_1$. By creating the velocity triangles, see Figure 2.2, it is easier to visualize the change of velocities and angles in a compressor stage (Saravanamutto, 2009).

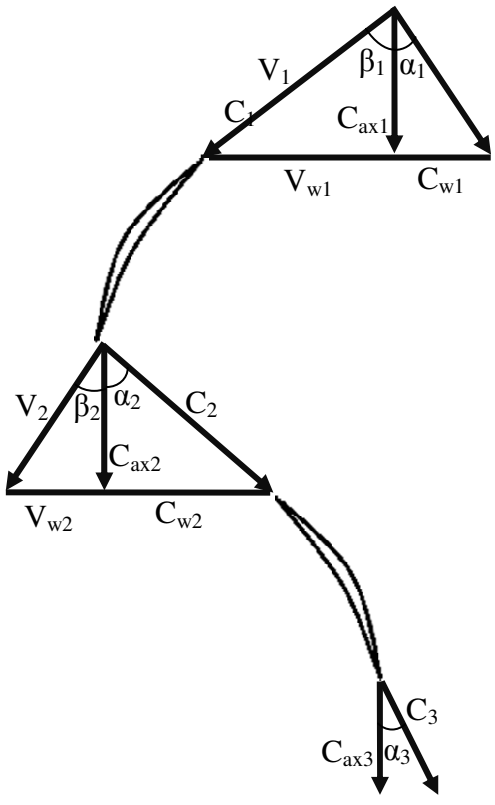

Figure 2.2 Velocity triangle for one stage

2.1.3 Stagnation Properties

If a gas is slowed down the kinetic energy will be transformed into internal energy to increase temperature and pressure. To include this kinetic energy in the enthalpy term of the moving fluid, stagnation (or total) properties are used which are defined as:

$$h_0 = h + \frac{C^2}{2} \tag{2.1}$$

Here h_0 is the stagnation enthalpy of the fluid, h is static enthalpy and C is the velocity of fluid. If the kinetic energy can be ignored, static enthalpy and total enthalpy is equal.

Similarly, if the moving fluid is a perfect gas, enthalpy, h, is equal to $T c_p$ so the stagnation temperature, T_0, is defined by

$$T_0 = T + \frac{C^2}{2c_p} \tag{2.2}$$

Here the second term, $\frac{C^2}{2c_p}$ is called the dynamic temperature which is illustrated in Figure 2.1, T is called static temperature and c_p is the specific heat value. Consider a compressor gas channel where through the gas channel gas speed is decreased but temperature and pressure are increased. In a similar way, stagnation pressure P_0 is defined with stagnation temperature under adiabatic and thermodynamically reversible condition. So the stagnation pressure for an ideal gas is given by

$$\frac{T_0}{T} = \left(\frac{P_0}{P}\right)^{\frac{\gamma-1}{\gamma}} \tag{2.3}$$

where γ, is the ratio between. Figure 2.1 shows the stagnation and static properties relationships for one stage.

2.1.4 Dimensionless Parameters

During the compressor design, a few dimensionless parameters such as the stage loading, the flow coefficient, the degree of reaction and the de Haller number play a key role to achieve a good compressor performance. Too aggressive pressure rise may drive the compressor into an unacceptable operating regime like stall or surge. (Dixon, 2010)

2.1.4.1 Stage Loading

The stage loading coefficient parameter, ψ, relates the compressor blade speed to the increase in specific enthalpy. The stage loading coefficient is defined as

$$\psi = \frac{\Delta h}{U^2} \tag{2.4}$$

Here Δh is the enthalpy difference and U is blade mid speed. (Dixon, 2010)

2.1.4.2 Flow Coefficient

The flow coefficient, ϕ, is another useful parameter. This parameter has so strong influence on performance and is defined as followed:

$$\phi = \frac{C_x}{U} \tag{2.5}$$

where C_x is the axial velocity. The flow coefficient and the stage loading affect each other through the velocity triangles. The relation can, with some simplifying assumptions be written as

$$\psi = \phi\left[\tan(\beta_1) - \tan(\beta_2)\right] \tag{2.6}$$

Equation 2.6 shows that for constant blade angles, increasing stage loading is equivalent to increasing the flow coefficient. This property is advantageous for reducing the engine size because a higher value of the flow coefficient leads to a higher inlet mass flow. However transonic effects limit this possibility. A high flow coefficient means a high Mach number and high Mach numbers causes fluid shocks. Typical values of ϕ is between 0.4 – 0.8 (Dixon, 2010).

2.1.4.3 Degree of Reaction

The general definition of the stage reaction, R, is the rise in static enthalpy in rotor compared to the rise in stagnation enthalpy throughout the stage.

$$R = \frac{h_2 - h_1}{h_{03} - h_{01}} \tag{2.7}$$

This parameter interrelates the diffusion in rotor to the stage diffusion. If the reaction is 1, the rotor would do all of the diffusion or static enthalpy rise. Similarly if the reaction is 0, the stator would do all of the diffusion or achieve all of the static enthalpy rise. Neither of these two extreme conditions lead to promising designs. In practice a higher degree of reaction is preferred that generally is selected in the range of 0.5 – 0.8 (Dixon, 2010).

2.1.4.4 de Haller number

The de Haller number is simply a measure of the amount of diffusion over the blade and is defined as follows:

$$\frac{V_2}{V_1} \geq 0.72 \tag{2.8}$$

here V_2 is the velocity at trailing edge of the blade and V_1 is the velocity at leading edge of it. This ratio is supposed to be not smaller than a pre-assumed limit. This limit is referred to as the de Haller limit number. In this work the value 0.72 is set to limit the diffusion. High whirl velocities means high fluid deflection and high fluid deflection means a high diffusion rate. Therefore the de Haller number is necessary to control the whirl velocity. If the de Haller number is small, the diffusion will be high.

2.1.4.5 Diffusion Factor

During the compressor design, the choice of the diffusion factor is critical. The air passing over an airfoil increases its speed on the leading part of the surface with an associated static pressure decrease. However as the air passes over the trailing part of the airfoil the fluid decelerates. As a result of this negative velocity gradient the boundary layer grows rapidly. A relatively thick boundary layers results from this process risking to cause a high degree of losses. The diffusion factor quantifies this process and is defined as:

$$DF = 1 - \frac{V_2}{V_1} + \frac{\Delta C_w}{2V_1}\frac{s}{c} \tag{2.9}$$

Here s is pitch of blade, c is chord of blade and ΔC_w is whirl velocity (Saravanamutto, 2009).

2.1.5 Thermodynamic Efficiency

The efficiency of a compressor is generally defined as:

$$\eta = \frac{power\ transfer\ in\ ideal\ process}{actual\ compressor\ power} \tag{2.10}$$

There are several types of efficiency definitions but in this study the isentropic and polytrophic efficiencies are used. These two efficiency types are the most widely used (Dixon, 2010).

2.1.5.1 Isentropic Efficiency

The isentropic efficiency of a compressor is defined as the ratio between the ideal work input to an isentropic process and the actual work input. It must not be forgotten that compressors essentially constitute an adiabatic The isentropic efficiency is defined as

$$\eta_c = \frac{W'}{W} = \frac{\Delta h_0'}{\Delta h_0} \tag{2.11}$$

For a perfect gas $\Delta h = c_p \Delta T$ and if this relation is applied the isentropic efficiency can be rewritten as:

$$\eta_c = \frac{T_{02}^{'} - T_{01}}{T_{02} - T_{01}} \tag{2.12}$$

here the variation of the c_p value with temperature is ignored because the ideal and actual temperature change is usually negligible (Saravanamutto, 2009).

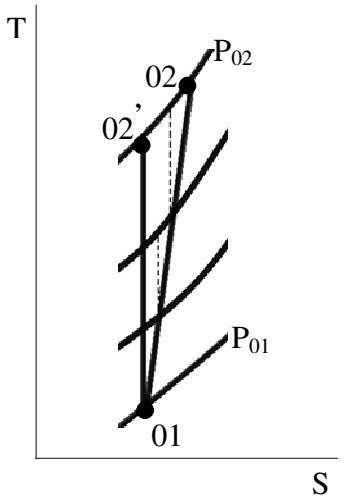

Figure 2.3 Compression process

Figure 2.3 represent a compression process T–s diagram of an engine for a given pressure rise. If the cycle is ideal, the temperature difference is taken from 01 to 02'. Otherwise, if the cycle is real, the temperature difference is represented as 01 to 02.

2.1.5.2 Polytrophic Efficiency

If it is considered that the whole compression is comprised of a large number of very small stages and each small stage has the same isentropic efficiency, see Fig. 3, the isentropic efficiency of the whole compressor is different from the small stage efficiency. For this reason the use of the isentropic efficiency can be misleading (Dixon, 2010). This consideration has lead to the need for the polytrophic or small stage efficiency, $\eta_{\infty c}$, which is defined by following equation (Saravanamutto, 2009).

$$\eta_{\infty,c} = \frac{\ln\left(\frac{P_2}{P_1}\right)^{\frac{\gamma-1}{\gamma}}}{\ln\left(\frac{T_2}{T_1}\right)} \tag{2.13}$$

2.2 Mechanical System

The mechanical system studied here is essentially equivalent to the gas generator. In other words it essentially consists of the LP rotor system and the HP rotor including bearings as well as bearing supports. The combustion system is also important to the mechanical design. Only the HPC system design is treated in some detail in this work, i.e. it defines the blade and disk designs, corresponding stress calculations and a rotordynamic system analysis.

2.2.1 Compressor Blades

The compressor blade is a rotating aerofoil on the disc of a compressor. This component of the engine transfers energy to the working fluid in order to increase its density and pressure. Appendix 1 gives an explanation of the cascade nomenclature used in this thesis.

2.2.2 Disc Design

Integrally bladed rotors (IBR), frequently referred to as bliscs, is a single engine component comprised of a rotor disk and blades. It was first used in the mid 1980s on helicopter engines (wikipedia). Due to not using any screws, bolts etc, the use of the blisc decreases the number of components inside the compressor as well as potentially its weight and cost. However in case of any damage on the blisc, the replacement of the entire blisc is may be necessary.

The stress analysis is focused on a blisc type design. The whole disc is considered as a superposition of several elementary computational parts like the ring, the hyperbolic section and a web type section. This calculation will be explained in the disk design and stress calculations within chapter 3.

2.2.3 Rotordynamic Theory

A rotordynamic analysis is made on the complete gas generator because the compressor system is only one part of the dynamic system; also there are turbines, bearings and bearing supports in the dynamic system. In order to get a high performance, high rotational speed is necessary and this will eventually due to asymmetry, unbalances or misalignments between components create dynamic loads in the engine (Saravanamutto, 2009).

Furthermore engine vibrations will be even more dangerous when the natural frequency of the whole system and the rotational speed frequency are equal. That speed is called *critical speed*, resonance then occurs and response of the system increases dramatically. So the designer needs to know where the critical speeds are.

To understand the behaviour of a mechanical system its stiffness and also its mass are needed. Both will affect the natural frequency. Equation 2.14 shows how it affects the system frequency.

$$f = \sqrt{\frac{k}{m}} \tag{2.14}$$

Increasing the stiffness (k) will result in increasing frequency (f). Increasing the mass of the system will lead to a decrease in frequency.

Rotors of compressors and turbines, bearings and their supports etc create a dynamic system and they affect each other. To understand this, consider a general linear system with constant coefficients. The equation of motion is

$$m\ddot{x} + c\dot{x} + kx = F_0 \cos \omega t \tag{2.15}$$

The general solution of this second order ordinary differential equation is a superposition of a homogeneous solution and a particular solution. The homogenous solution gives the *free vibration* or *natural motion* behaviour of the system and is obtained by the elimination of the force term.

A particular solution is obtained by applying a force, such as $F_0 \cos \omega t$. A forced response is called *forced vibration* or *steady state response.* In free vibrations no energy is exchanged with the environment, while in a forced vibration there is an energy exchange (Chen & Gunter, 2007).

Free vibration occurs naturally with no energy being added to the vibrating system. Vibration is started by a given initial disturbance (input of energy) to the system. This initial disturbance source may originate either from a displacement of the mass, an initial velocity of the mass or both. Thereafter all the forces, all the moment of force acting or all initial disturbances on the body must add up to zero. So vibrations die away with time as the energy is dissipated. Because there is a natural force that tries to return the system its initial state (Chen & Gunter, 2007).

There are many types of excitations that are encountered in rotating machinery. Steady state unbalance response is the most common. Disk skew and shaft bow are the most common source of excitation in the rotating machine. No matter how well they are balanced, the rotors always have some amount of residual unbalance. The frequency of the unbalance excitation, that is a harmonic excitation, is synchronized with the rotational speed. Therefore *steady state response* is frequently referred to as *synchronous excitation*. Equation 2.15 is shows the differential equation of motion of a single degree of freedom system with harmonic excitation (Chen & Gunter, 2007).

The *Campbell diagram* is normally used to describe the *damped critical speed* and it represents the systems response spectrum. The Campbell diagram is a plot of damped natural frequencies of the rotating system. In rotor dynamics, natural frequencies are sometimes called *whirl speeds.* A "*Whirl speed map*" or "*frequency interference diagram*" is generally a synonym for a "Campbell Diagram" (Chen & Gunter, 2007).

3 Methodology

According to Figure 1.1, the multidisciplinary compressor design process can start with determining the requirements of a high pressure compressor. After preparation of the design procedure, the thermodynamic cycle analysis is started. The thermodynamic cycle design gives preliminary input to aerodynamic design like pressure ratios, temperatures and mass flows. Then, the preliminary aerodynamic design to obtain the number of stages, the rotational speed and geometric information of size of compressor etc is commenced. Finally, the mechanical design must be started using output of the prior analysis. There is always a feedback between all design steps. In addition, these three design steps are supported by material science, manufacturing, test and control departments. This multidisciplinary effort is referred to as Integrated Product Development (IPD). In this chapter specification to design, thermodynamic and aerodynamic analysis theory and mechanical design procedure theory of the High Pressure Compressor (HPC) is presented..

3.1 Design Specification

Some input for the HPC design comes from the Low Pressure Compressor (LPC) exit interface such as compressor inlet temperature, pressure, mass flow. These parameters help to specify the geometry and operating condition for the compressor.

To design an axial compressor one must define the flow path type of the compressor; for instance a constant outer (or tip) diameter, a constant mean diameter or a constant inner (or hub) diameter may be used. All geometries have some advantages and disadvantages. A Constant Mean Diameter (CMD) type compressor was preferred for this study.

The basic design parameters used in this work are presented in Table 3.1 as obtained from the LPC outlet and the engine performance specification. These values are used to generate the main geometry and operating conditions of the compressor.

Table 3.1 Input parameters for calculation

	Value
Inlet temperature	401.45 K
Inlet pressure	132.86 kPa
Mass flow	14.18 kg/s
Overall pressure ratio	4.46

If the axial velocity is set to be constant throughout the compressor, the blades at the end of the compressor will be very short and thus have higher losses and be more susceptible to mechanical stresses. Setting the Axial Velocity Ratio will take this into consideration.

3.2 Thermodynamic and Aerodynamic Design

This subsection reviews the elementary theory of thermodynamic and aerodynamic design in this work. To make a preliminary thermodynamic and aerodynamic conceptual design, a MATLAB algorithm was written. To obtain a general picture of the compressor, this code was used with certain requirements and assumptions to reach certain results. The equations used are listed in appendix 2.

3.3 Mechanical Design

3.3.1 Blade Design

The traditional approach to axial flow compressor aerodynamic design was to use families of airfoils. As design requirements began to support transonic flow, Double Circular Arc (DCA) blades became popular. Experimental cascade testing of DCA airfoils is relatively extensive so the performance characteristics of this airfoil family is relatively well understand (Aungier, 2003). For this reason the DCA airfoil was used. Figure 3.1 illustrates the general DCA profile.

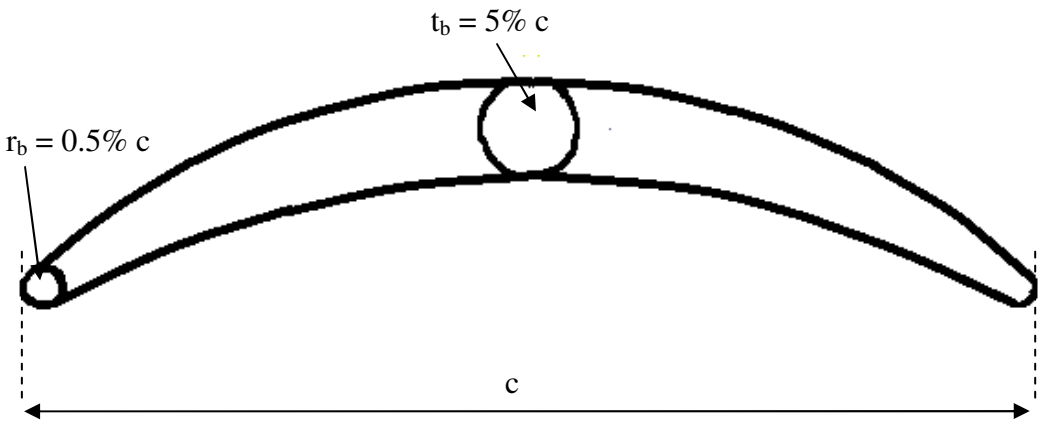

Figure 3.1 Double – Circular – Arc (DCA) airfoil profile

The DCA profile is developed with both surfaces formed by circular arcs. At both the leading and trailing edges the radius is r_0 and the upper and lower surface arc radii are R_U and R_L. R_C is the radius of the camber line curvature (Aungier, 2003). t_b and r_b were decided as respectively 5% and 0.5% of the chord for creating the airfoil arc, and the reason for this is essentially practical i.e. it is not practical to manufactur or even operate a HP compressor having too sharp trailing edges. If r_b is more than 0.5% of the chord, losses due to shocks are increased. If r_b is less than 0.5% of the chord, the blade will be very sensitive to foreign object damage will and manufacturing cost will increase. A t_b around 5% is also suitable because it will keep vibration and flutter problems down.

3.3.2 Free Vortex Calculation

Free vortex is used to determine variation of air angles from hub to tip. Up to now all calculations are at mid radius but to describe the variation of the air angles some aerodynamic result at hub and tip radius must be used. A free vortex design makes it possible to estimate the conditions at blade hub and tip. Assuming a constant specific work and constant axial velocity distribution along the blade height it can be shown that:

$$C_w r = constant \tag{3.1}$$

Using this approach, it is a simple matter to obtain some aerodynamic parameters like the de Haller number or the Mach number at the hub or the tip. However it should be kept in mind that the free vortex condition is associated with some disadvantages. In a real case blade un-twist will impact the initial definitions. This will require variations to the free vortex numbers.

In this design there is no any IGVs being used; this means there is no entry swirl and the inlet velocity will be constant across the annulus. For all other stages whirl velocity at the entry of the compressor rotor blades influence the flow angles. Keeping with the notation used for the velocity triangles in Figure 2.2, the rotor blade angle, $\beta_{1,}$ at any radius is obtained as:

$$\tan \beta_{1x} = \frac{U_x}{C_{ax}} \tag{3.2}$$

Here, x indicates the radius of the blade, i.e. hub, mid or tip radius. For first stage α_1 is equal to zero at three locations. After the first stage, α_1 is equal to the stator exit angle. To calculate the air angles β_1 and α_1 it is necessary to calculate the whirl speed, C_{w2}, at all 3 locations. From the free vortex condition,

$$C_{w2x} = C_{w2} \frac{r_{mid}}{r_x} \tag{3.3}$$

Also, stator inlet angle and rotor exit angle is calculated as:

$$\tan \alpha_{1x} = \frac{C_{w2x}}{C_{ax}} \tag{3.4}$$

$$\tan \beta_{1x} = \frac{U_x - C_{w2x}}{C_{ax}} \tag{3.5}$$

3.3.3 Disc Shapes and Stress Calculations

Disc shapes are based on stress calculations. The stress analysis is done by applying two methods. One of them uses basic analytic methods to create a model of the blisc and the other one uses a commercial software program, ANSYS, after making a model of the blisc to check the stresses. While creating a preliminary blisc model by using the analytic approach, the whole disc is considered as superposition of several

elementary parts such as the ring, the hyperbolic and the web shape. A second order differential equation can be defined to describe all the elementary shapes. The equation is derived by considering force equilibrium. From this, a stress-strain relation is obtained. Finally using boundary conditions, the equation is completely defined.

3.3.3.1 Equation of Equilibrium

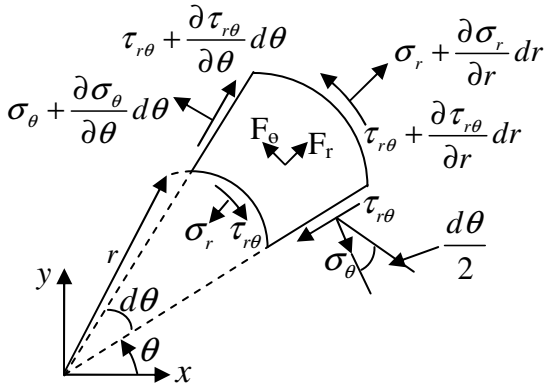

Figure 3.2 Stress elements in polar coordinates

Geometrical considerations often make it preferable to employ polar coordinates rather than the Cartesian system. In general, polar coordinates are preferred where a degree of axial symmetry exists such as a rotating disk. Figure 3.2 shows a unit element and its stress distribution under the condition of unit thickness. F_r and F_Θ and represent a directed body force. Equilibrium in the radial direction is:

$$\begin{aligned} F_r\ r\ dr\ d\theta+\left(\sigma_r+\frac{\partial\sigma_r}{\partial r}dr\right)(r+dr)\mathrm{d}\theta-\sigma_r r d\theta+\left(\tau_{r\theta}+\frac{\partial\tau_{r\theta}}{\partial\theta}d\theta\right)\mathrm{dr}\ \cos\frac{d\theta}{2} \\ -\tau_{r\theta}dr\cos\frac{d\theta}{2}-\left(\sigma_\theta+\frac{\partial\sigma_\theta}{\partial\theta}d\theta\right)dr\sin\frac{d\theta}{2}-\sigma_\theta dr\sin\frac{d\theta}{2}=0 \end{aligned} \tag{3.6}$$

and equilibrium in the tangential direction is:

$$\begin{aligned} F_\theta\ r\ dr\ d\theta+\left(\sigma_\theta+\frac{\partial\sigma_\theta}{\partial\theta}d\theta\right)dr-\sigma_\theta dr\cos\frac{d\theta}{2}+\left(\tau_{r\theta}+\frac{\partial\tau_{r\theta}}{\partial\theta}d\theta\right)(\mathrm{r+dr})\mathrm{d}\theta \\ -\tau_{r\theta}rd\theta+\tau_{r\theta}dr\sin\frac{d\theta}{2}+\left(\tau_{r\theta}+\frac{\partial\tau_{r\theta}}{\partial\theta}d\theta\right)dr\sin\frac{d\theta}{2}=0 \end{aligned} \tag{3.7}$$

Here, using small angle simplifications $\sin\frac{d\theta}{2}\cong\frac{d\theta}{2}$ and $\cos\frac{d\theta}{2}\cong 1$, finally the equilibrium equation for a disc is obtained as:

$$\frac{\partial\sigma_r}{\partial r}+\frac{\sigma_r-\sigma_\theta}{r}+\frac{1}{r}\frac{\partial\tau_{r\theta}}{\partial\theta}+F_r=0 \quad \text{(radial direction)} \tag{3.8}$$

$$\frac{\partial \tau_{r\theta}}{\partial \theta} + \frac{2\ \tau_{r\theta}}{r} + \frac{1}{r}\frac{\partial \sigma_{\theta}}{\partial \theta} + F_{\theta} = 0 \qquad \text{(tangential direction)} \tag{3.9}$$

3.3.3.2 Disc Geometry

Under plane stress conditions ($\sigma_z = 0$) the stresses are clearly symmetric around the z-axis. The centrifugal inertia force, $F=\rho w^2 r$, create the body force F_r. Also, disc stresses are assumed to be distributed symmetrically in the tangential direction of the disc so deformations are independent of the Θ direction. The symmetry reveals that shearing stresses $\tau_{r\Theta}$ must be zero. So equation 3.8 can be written as:

$$\frac{\partial \sigma_r}{\partial r} + \frac{\sigma_r - \sigma_{\theta}}{r} + \rho w^2 r = 0 \qquad \text{(radial direction)} \tag{3.10}$$

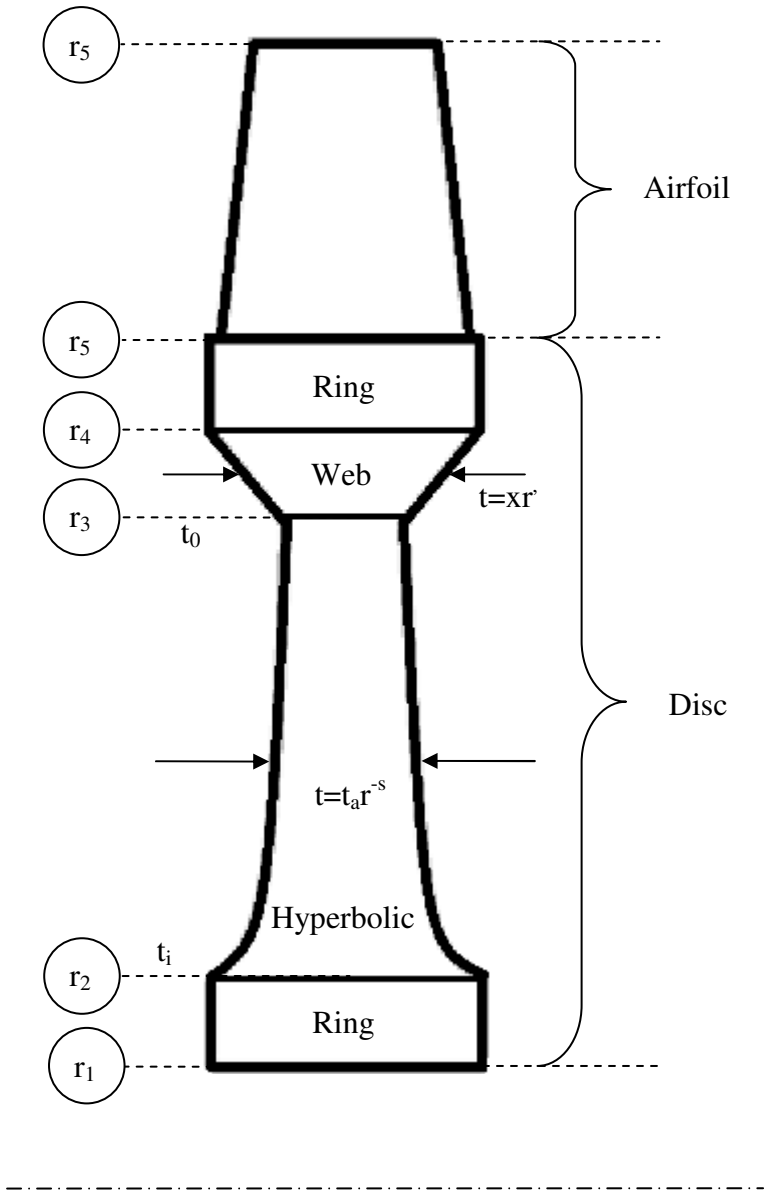

Figure 3.3 Geometry and part of blisk shape and radial stations

Rotating Disc of Constant Thickness

Along the ring shape, thickness is constant and thermal stresses are neglected. Solving the Cauchy – Euler Differential equation provides the following equation for radial and tangential stress:

$$\sigma_r = \frac{E}{1-\upsilon^2}\left((1+v)c_1 - (1-v)\frac{c_2}{r^2} - \frac{(1-v^2)(3+v)\rho w^2 r^2}{8E}\right) \tag{3.11}$$

$$\sigma_\theta = \frac{E}{1-\upsilon^2}\left((1+v)c_1 + (1-v)\frac{c_2}{r^2} - \frac{(1-v^2)(1+3v)\rho w^2 r^2}{8E}\right) \tag{3.12}$$

here c_1 and c_2 are constants of integration that are evaluated based on boundary conditions. At station r_1 the radial stress is 0. At station r_2 the radial stress of the ring geometry is equal to a hyperbolic shape radial stress.

Rotating Disc of Variable Thickness

A hyperbolic geometry is considered as a second part of the disc definition (Figure 3.3). The thickness of general hyperbolic geometry is described by

$$t = t_a r^{-s} \tag{3.13}$$

here t_a is constant and s is positive number and the shape of the curve depends on value of s. If the thickness t_i occurs at station r_2 and the thickness t_0 occurs at station r_3, the resulting hyperbolic curve is obtained by:

$$s = -\frac{\log\left(\frac{t_i}{t_0}\right)}{\log\left(\frac{r_2}{r_3}\right)} \tag{3.14}$$

Under variable thickness conditions, the equation of equilibrium must include $t(r)$ and is rewritten as:

$$\frac{d}{dr}(tr\sigma_r) - t\sigma_\theta + t\rho w^2 r^2 = 0 \tag{3.15}$$

If solved, this equation of equilibrium produces the stress components:

$$\sigma_r = \frac{c_1}{t_a} r^{m_1+s-1} + \frac{c_2}{t_a} r^{m_2+s-1} - \frac{3+v}{8-(3+v)s}\rho w^2 r^2 \tag{3.16}$$

$$\sigma_\theta = \frac{c_1}{t_a} m_1 r^{m_1+s-1} + \frac{c_2}{t_a} m_2 r^{m_2+s-1} - \frac{1+3v}{8-(3+v)s}\rho w^2 r^2 \tag{3.17}$$

where c_1 and c_2 can be determined from the boundary conditions. The boundary conditions at the r_2 and the r_3 points are defined by having the same tangential stress value.

Web shape

Within the web shape section the thickness changes as a linear function according to:

$$t = mr' \tag{3.18}$$

Here m is a constant that describes the slope of the web.

So using same equation of equilibrium and solution technique, stress components for the web shape can be found as:

$$\sigma_r = \frac{c_1}{m^{x_1-1}}(mr+b)^{x_1-2} + \frac{c_2}{m^{x_1-1}}(mr+b)^{x_2-2} - \frac{3+v}{(v+11)m^2}\rho w^2 (mr+b)^2 \tag{3.19}$$

$$\sigma_\theta = \frac{c_1}{m^{x_1-1}}x_1(mr+b)^{x_1-2} + \frac{c_2}{m^{x_1-1}}x_2(mr+b)^{x_2-2} - \frac{1+3v}{(v+11)m^2}\rho w^2 (mr+b)^2 \tag{3.20}$$

here c_1 and c_2 are determined by applying boundary conditions.

3.3.4 Rotordynamic System

The rotordynamic analysis includes the complete gas generator system. Therefore the geometry of the other components of the gas generator is required. The HPC geometry information stems from the aerodynamic analysis. Geometry data of turbine comes from the Chalmers in-house simulation program WEICO. After using the DyRoBeS software program, all gas generator critical speeds, mode shapes and displacements can be obtained. Bearing stiffnesses have been calculated based on rough dimensions of conventional SKF roller bearings.

4 Results

The previous chapters have tried to present the aim of this master thesis, some basic relationships and applications of these relationships. In this chapter, a preliminary mean-line HP compressor thermodynamic, aerodynamic and mechanical design will be presented. During this process, MATLAB is used for aerodynamic and thermodynamic calculations in order to obtain the preliminary geometry of the HP compressor. CATIA V5R16 is used for creating the 3D model of the blisc and ANSYS13 is used for the structural analyses. The DyRoBeS program is subsequently used for the rotor dynamic analysis of the whole gas generator.

4.1 Thermodynamics and Aerodynamics

Table 3.1 presents some input parameters. These input parameters come from the LP compressor exit values and the cycle design conditions. The design criteria applied is to obtain minimum mission fuel burn. The aerodynamic design point selected is the top–of–climb point because generally aircraft engines have to have maximum power during takeoff but they have the maximum aerodynamic loading at top-of-climb.

The HP compressor is assumed to be of constant mid radius, it has a mass flow of 14.18 kg/s and a pressure ratio on the HP compressor is 4.46. To reach this pressure ration the HP compressor needs 5 stages. Table 4.1 summarises the main specifications of the HP compressor.

Table 4.1 main specification of HP compressor

Main specification	**Value**
Type of compressor	Constant Mean Diameter (CMD)
Inlet temperature	401.452 K
Inlet pressure	132.862 kPa
Mass flow	14.1832 kg/s
Number of stages	5
Rotational speed	2104.5 rad/s (335.09rms)
Inlet axial velocity	177.17 m/s
Inlet axial mach number	0.35
Inlet relative mach number	1.28
Inlet hub – tip ratio	0.72
Inlet air angle	0^o
Exit air angle	0^o

Table 4.1 presents initial conditions and compressor exit conditions. The first step in the aerodynamic conceptual design process is to define stage by stage data. This process is constrained by a number of conditions such as maximum flow factors, stage loadings and diffusion factors. The process is similar to an optimization process where a large number of designs are evaluated. The stage by stage values are listed below in table 4.2. Values are given at stage outlets. The parameters at the inlet of the HP compressor are the same as the parameters estimated at the outlet of the LP compressor.

Table 4.2 Detailed calculations

	T_0 (K)	P_0 (kPa)	C_{ax} (m/s)	M	ρ (kg/m^3)
Inlet of HPC	401.45	132.86	177.18	0.45	1.04
1st stage	449.07	188.04	172.75	0.42	1.33
2nd stage	498.33	260.52	169.30	0.39	1.68
3rd stage	548.41	351.65	164.22	0.36	2.09
4th stage	598.49	462.27	163.89	0.35	2.53
5th stage (exit of HPC)	646.11	585.98	163.48	0.32	3.00

The velocity triangles of the HP compressor are given in Table 4.3. First stage inlet air angle (α_1) and last stage exit air angle (α_3) are zero.

Table 4.3 Velocity triangles of the HP compressor at mean line

	α_1	β_1	α_2	β_2	C_1	V_1	C_2	V_2	de Haller number rotor	de Haller number stator	ψ
1st stage	0	66.43	33.62	58.44	177.18	443.18	212.77	338.50	0.77	0.84	0.58
2nd stage	14.00	64.56	43.67	54.40	178.04	402.15	238.85	296.75	0.74	0.73	0.60
3rd stage	14.00	65.06	44.45	54.81	174.49	401.46	237.18	293.80	0.73	0.72	0.61
4th stage	15.92	65.44	46.11	55.11	170.77	395.13	236.90	287.09	0.73	0.72	0.61
5th stage	16.08	65.46	45.20	55.80	170.56	394.62	232.60	291.59	0.74	0.70	0.58

Note that the last stage de Haller number is 0.70 which is below the initial assumptions. It is however believed that it is possible to design for a de Haller number of 0.70 without compromising compressor efficiency. The HP compressor isentropic efficiency is estimated as 0.8797 and the polytrophic efficiency is 0.9020. These efficiencies are calculated by using a Chalmers in-house code for estimating compressor losses [Xu, 2011]. The code uses empirically based correlations, primarily the Miller and Wright compressor model [1991].

Table 4.4 Geometric parameters of the HP compressor's rotor

	r_{hub} (mm)	r_{tip} (mm)	N	$\eta_{\infty c}$	η_c
Inlet of HPC	161.3	224.6			
1st stage	167.7	218.3	46	0.8970	0.8919
2nd stage	172.6	213.3	54	0.9056	0.9011
3rd stage	176.1	209.8	59	0.9056	0.9014
4th stage	179.1	206.8	65	0.9049	0.9011
5th stage (exit of HPC)	181.2	204.7	72	0.8967	0.8931

Geometry parameters of blades are presented in Table 4.5. These parameters are calculated using the WEICO design code. Twist angles are calculated by using the free vortex calculation method.

Table 4.5 Geometry parameters of HP compressor's rotor

	Chord (mm)	Thickness (mm)	Twist angle (hub–mid) at le	Twist angle (tip–mid) at le
1st stage	30.6	1.53	3.98	3.02
2nd stage	28.4	1.42	4.21	3.15
3rd stage	26.2	1.31	3.71	2.55
4th stage	25.3	1.27	2.65	2.17
5th stage	24.0	1.25	2.15	1.82

The thickness numbers refers to the mid of blade where the blade has a maximum thickness. It is shown in Figure 4.1, below.

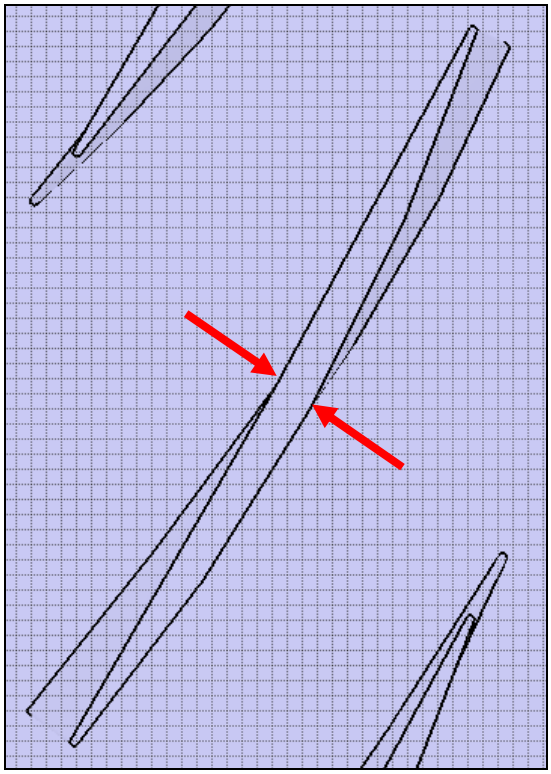

Figure 4.1 Maximum blade thickness

For obtaining a first design of the disc geometry the WEICO code was used. The resulting data are presented in appendix 3.

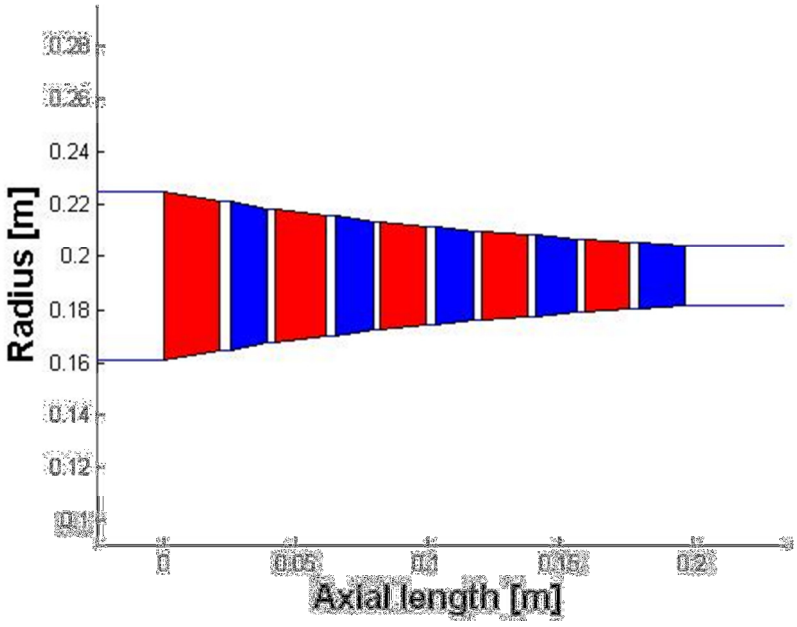

Figure 4.2 Compressor geometry

4.2 Stress Analysis

In this master thesis presents two different stress calculation procedures. The first uses an analytic based stress calculation as described previously. The second method uses the ANSYS software. The purpose of this activity is to compare the two methods.

The Double Circular Arc (DCA) airfoil is selected for blade shape determination. Figure 3.1 shows the DCA airfoil and its dimensions. Three radii's are selected to draw the airfoil shape; at the hub, the mid and the tip. Then, the DCA profile is drawn at these 3 radii including twist angles that are calculated using the free vortex model. These are presented in Table 4.5. The increment angle is assumed to be 5^{o} for a first draft of the design process.

After the aerodynamic analysis, blade shape and disc geometry was obtained. The 3D modelling was performed in the CATIA software to model the rotor blisc shape. Appendix 4 shows all five stages with CATIA drawings.

For creating an ANSYS model, the blade and the blisc were assigned the materials Ti17 and Inco718. The material properties are based on the temperature values. For temperatures greater than 644.4 K, Inco718 and below this temperature limit Ti17 is used. For the first three blade rows Ti17 is used, and for the last two blade rows Inco718 is applied. The mechanical properties are shows in Table 4.6.

Table 4.6 Mechanical properties of material

		Ti17	**Inco718**
Density	kg/m^3	4510	8220.96
Young's Modulus	GPa	115	200
Poisson ratio		0.33	0.29
Coefficient of thermal expansion	$1/^{o}C$	$9.4x10^{-6}$	$13.55x10^{-6}$
Reference temperature	^{o}C	22	204
Isotropic thermal conductivity	$W/m^{o}C$	7.80	11.4

Using the above mentioned properties of the material for the blade and disc, results from the ANSYS analysis for a pre-determined temperature distribution can be studied. Von Mises stresses and the strain of the blisc, both under the thermal and non-thermal effects at a rotational speed of 2104.5 rad/s can be found. The resulting temperature distributions are shown in Table 4.7 and in appendix 5 according to Figure 4.3.

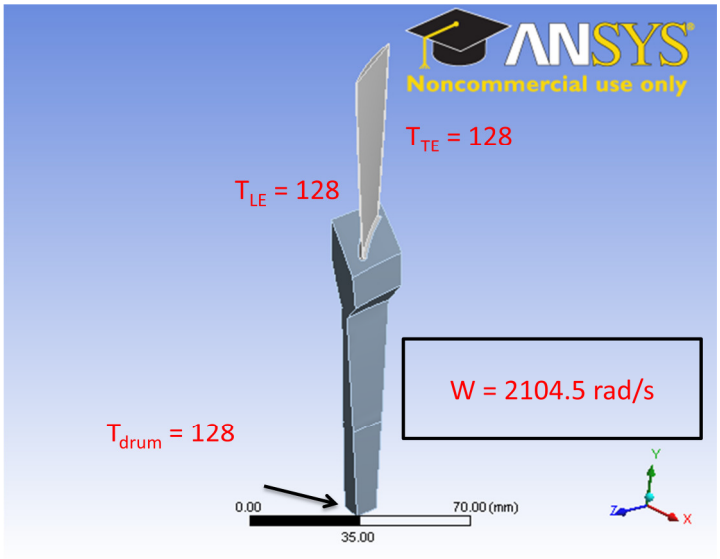

Figure 4.3 Loads for numerical ANSYS model (1 blade Blisc – 1st stage)

Table 4.7 Mechanical properties of the material

	T_{LE} (C^0)	T_{TE} (C^0)	T_{DRUM} (C^0)	w (rad/s)
1st stage	128	176	128	2104
2nd stage	176	225	128	2104
3rd stage	225	275	128	2104
4th stage	275	325	128	2104
5th stage	325	373	128	2104

For the temperature distribution the ANSYS model has three temperatures; at the leading edge, the trailing edge and the drum temperature. The drum temperature is the same as the first stage inlet temperature. The temperature at the trailing edge is higher than the leading edge and drum temperatures.

The analytic stress calculation procedure was used to establish the disc geometry. Figure 3.3 shows the geometry of blisc. The stress calculation is done at five stations; the ring, the hyperbolic shape the web shape and finally another ring shape as shown in Figure 3.3. By using equations 3.11, 3.12 for the ring shape and equations 3.16 and 3.17 for hyperbolic shape σ_r and σ_Θ can be calculated. If the calculated values of σ_r and σ_Θ are the same for both the ring and hyperbolic shapes then this shows that the design process has converged for this interface. Similarly, the geometric shape of the web is determined by comparing the results of equation 3.16 and 3.17 with 3.19 and 3.20 at radius r_3. Calculations for r_4 is done by comparing the results from equations 3.11 and 3.12 with equation 3.19 and 3.20 which will give the second ring shape. r_5 is same as r_{hub} of the blade. The WEICO stress results are shown in Table 4.8.

Table 4.8 von Mises stress calculation results by using theoretical equation in the stations

Station number	1st stage	2nd stage	3rd stage	4th stage	5th stage
1	521	521	521	521	521
2	317	339	355	367	375
3	225	222	214	214	210
4	205	202	198	199	197
5	188	186	184	187	186

Also, the von Mises stresses were calculated using ANSYS and for this calculation the WEICO blisc geometry result was used. ANSYS results are presented in appendix 4. In Table 4.9 numerical results are shown for the von Mises stresses with a constant temperature distribution. Table 4.10 shows numerical results of von Mises stresses with a temperature distribution.

Table 4.9 von Mises stress results (MPa) computed using the ANSYS software (constant temperature distribution)

Station number	1st stage	2nd stage	3rd stage	4th stage	5th stage
1	455	450	415	950	990
2	300	340	320	700	515
3	290	300	200	450	400
4	150	165	153	275	275
5	140	150	140	240	250

Table 4.10 von Mises stress calculation results (MPa) using the ANSYS software (including a linear temperature distribution)

Station number	1st stage	2nd stage	3rd stage	4th stage	5th stage
1	530	570	550	1104	1110
2	340	380	400	750	780
3	285	300	280	400	590
4	120	125	90	50	10
5	110	100	80	40	16

In Table 4.11 to Table 4.15 data for every blisc station are given showing the von Mises stresses and Yield Stresses.

Table 4.11 1st HPC blisc ANSYS results and Yields strength at the blisc stations

radius	WEICO	ANSYS Without T	ANSYS With T	Yield Strength
62	521	455	530	1050
94	317	300	340	1050
137	225	290	285	1050
149	205	150	120	1050
162	188	140	110	1050

Table 4.12 2nd HPC blisc ANSYS results and Yields strength at the blisc stations

radius	WEICO	ANSYS Without T	ANSYS With T	Yield Strength
64	521	450	570	1050
91	339	340	380	1050
142	222	300	250	1050
155	202	165	125	1050
168	186	150	100	1050

Table 4.13 3rd HPC blisc ANSYS results and Yields strength at the blisc stations

radius	WEICO	ANSYS Without T	ANSYS With T	Yield Strength
66	521	415	550	1050
89	355	320	400	1050
150	214	210	280	1050
161	198	153	90	1050
174	184	140	80	1050

Table 4.14 4th HPC blisc ANSYS results and Yields strength at the blisc stations

radius	WEICO	ANSYS Without T	ANSYS With T	Yield Strength
67	521	950	1104	1035
88	367	700	750	1035
156	214	450	400	1035
166	199	275	50	1035
176	187	240	40	1035

Table 4.15 5th HPC blisc ANSYS results and Yields strength at the blisc stations

radius	WEICO	ANSYS Without T	ANSYS With T	Yield Strength
68	521	990	1110	1035
87	375	515	780	1035
160	210	400	590	1035
169	197	275	10	1035
180	186	250	16	1035

Because of the rotational velocity and centrifugal stresses the rotor blades expand and impact the tip clearances. Table 4.16 shows the blade height and the amount of strain.

Table 4.16 Computed Tip clearances with constant and linear temperature distributions using the ANSYS software

(mm)	h (mm)	Without T (mm)	With T (mm)
1st stage	63.2	0.86	0.95
2nd stage	50.5	0.56	0.73
3rd stage	40.6	0.32	0.59
4th stage	33.7	0.27	0.77
5th stage	27.8	0.25	0.83

4.3 Rotordynamic Analysis

A preliminary and somewhat rough rotor dynamic analysis is outlined for the complete gas generator i.e. both the LP rotor and the HP rotor. In appendix 7 the geometry of a complete DyRoBeS model of the gas generator is shown. Although the LP rotor is mechanically independent of the HP rotor both are linked to one another aerodynamically. The relatively long and slender LP rotor is supported by three (roller) bearings and the HP rotor by two (roller) bearings.

The objective of the *Eigen frequency analysis* is to calculate all relevant Eigen frequencies of the rotor dynamic system and thereby identify critical speeds near the operating range of the gas generator. At an early stage of a new project it is often a good idea to also include higher Eigen frequencies (i.e. well beyond the upper limit of the rotor speeds) to get a rotor dynamic "overview". A Campbell diagram showing all calculated Eigen frequencies versus rotor speed up to 60000 rpm can be found in Appendix 8. Calculated Eigen frequencies will diverge more or less strongly depending on how strong the gyroscopic influence is. Increasing Eigen frequencies represent so called forward whirl and decreasing Eigen frequencies represent back-ward whirl. In this context only forward whirling modes are of interest. Only unbalance critical speeds which are characterized forward whirling modes are considered here.

To each critical speed it is possible to identify a vibration mode or "shape". Typically these "shapes" will deviate considerably from one another. However, sometimes they are very similar which could make it difficult to establish a "positive identification" if these critical speeds are close. Relevant Eigen frequency modes have been calculated and are presented in Appendix 9. There are altogether five critical speeds within or near the operating speed of the LP rotor and HP rotor respectively. The vibration mode (or "shape") which is associated to each critical speed is presented in a relative scale.

Note that the mode shapes which will result from an Eigen frequency analysis are approximate or more precisely the mode shapes are given in a relative scale.

Contrary to an Eigen frequency analysis the outcome of a response analysis will give the radial displacement of a rotor along its axis in absolute terms (i.e. in m or mm).

However, a *response analysis* requires more input information like an unbalance distribution and damping (without any damping at the rotor supports the rotor displacement will actually be infinite in theory). Note that even if there is no (viscous) damping device included in the turbo machinery there will always be some damping due to vibration energy dissipation in the engine stator structure.

In Appendix 10 the results of a response analysis is presented. Local rotor displacements are given at two different axial stations (stn x and stn y).

By assuming a typical axial unbalance distribution along each rotor the radial displacement can be calculated as function of rotor speed at different axial stations (or elements) of the rotordynamic model. No relative phase difference between individual unbalance force vectors plus a low (equivalent) viscous damping has been used in the underlying response analysis.

Both the Eigen frequency analysis and the response analysis indicate that there are four critical speeds in or very near the operating speed range. Furthermore there is also a fifth critical speed around 34500 rpm which may seem sufficiently far away from the operating range to be neglected. However it is included since future design modifications may easily change this situation. A summary of all the five critical speeds are given in Table 4.17 below.

Table 4.17 Critical speed results of DyRoBeS software

	Critical Speeds (rpm)
1st LP rotor	11065
2nd LP rotor	12776
3rd HP rotor	15937
4th LP rotor	16837
5th HP rotor	34516

5 Conclusions

5.1 Aerodynamics

An aerodynamic analysis gives the outline of a five stage HP compressor which will have the theoretical capability of enabling a high efficiency gas generator performance.

5.2 Mechanical Design

All the HP compressor stages are “bliscs” which are assembled by friction welding according to well known and established manufacturing processes.

The blade shape is very especially thin at the leading and trailing edges which contributes to achieving a high aerodynamic efficiency with low losses. However the curvature radius at the leading and trailing edge is sufficiently great to allow acceptable manufacturing costs.

5.3 Stress Analyses

A comparison between the WEICO stress analysis model and the 3D ANSYS model shows that there is some difference in calculated radial and tangential stresses. Without further analysis this is attributed to the stress concentrations occurring in a 3D model. In the analytic model the blade pull stresses are smeared uniformly over the periphery of the disc. If the temperature distribution is taken into account then the stress levels are actually approaching the levels obtained by the simple WEICO model.

Calculating the von Mises equivalent stresses shows that safety factor is between 1.2 and 1.8 for all HP compressor stages. It should be pointed out that in practice critical conditions for disc design is not always stress based, but sufficient stiffness is needed which WEICO includes as minimum disc thickness values. No such vibration analysis has been performed within this theses so an analysis whether this assumptions are realistic is viewed as future work.

5.4 Rotordynamics

A rotordynamic analysis covering rotor speeds up to 60000 rpm indicates that there are 4 critical speeds within the operating range (maximum speed 20100 rpm). In addition to that, a response analysis based on a typical unbalance distribution gives rotor displacements which are less than 2 mm. Damping of the system is based on a very rough estimate which is approximately equal to a typical structural (material) damping.

6 References

Aungier, R.H., Axial – Flow Compressors: A Strategy for Aerodynamic Design and Analysis, New York, Asme Press, 2003

Aungier, R.H., Turbine Aerodynamics: Axial Flow and Radial Inflow Turbine Design and Analyses, US, Asme press, 2006

Dixon, S.L., Hall, CA., Fluid Mechanics and Thermodynamics of Turbomachinery (6th Ed.), Elsevier, 2010

L. Xu, Analysis and Evaluation of Innovative Aero Engine Core Concepts, PhD Thesis, Chalmers University and Technology, 2011

Saravanamutto, H.I.H., Rogers, GFC., Cohen, H., Straznicky, PV., Gas Turbine Theory (6th Ed), Pearson Prentice Hall, 2009

Ugural, AC., Fenster, AK., Advanced Strength and Applied Elasticity (3rd Ed.), Prentice Hall PTR, New Jersey, 1995

Wilson, D.G., Korakianitis, T., The Design of High - Efficiency Turbomachinery and Gas Turbines (2nd Ed.), US, Prentice Hall, 1998

Wilson, D.G., The Design of High-Efficiency Turbomachinery and Gas Turbines (5th Ed.), MIT press, 1991

Wright, P. I. and Miller, D. C., "An Improved Compressor Performance Prediction Model," No. C423/028, 1991.

Appendix

Appendix 1

aspect ratio: the ratio of the blade height to the chord.

axial chord: the length of the projection of the blade, as set in the turbine, onto a line parallel to the turbine axis. It is the axial length of the blade.

axial solidity: the ratio of the axial chord to the spacing.

blade exit angle: the angle between the tangent to the camber line at the trailing edge and the turbine axial direction.

blade height: the radius at the tip minus the radius at the hub.

blade inlet angle: the angle between the tangent to the camber line at the leading edge and the turbine axial direction.

camber angle: the external angle formed by the intersection of the tangents to the camber line at the leading and trailing edges. It is equal to the sum of the angles formed by the chord line and the camber-line tangents.

camber line: the mean line of the blade profile. It extends from the leading edge to the trailing edge, halfway between the pressure surface and the suction surface.

chord: the length of the perpendicular projection of the blade profile onto the chord line. It is approximately equal to the linear distance between the leading edge and the trailing edge.

chord line: if a two-dimensional blade section were laid convex side up on a flat surface, the chord line is the line between the points where the front and the rear of the blade section would touch the surface.

compressor: a rotary machine that produces a relatively high pressure rise (pressure ratios greater than 1.1) in a compressible fluid.

deflection: the total turning angle of the fluid. It is equal to the difference between the flow inlet angle and the flow exit angle.

deviation angle: the flow exit angle minus the blade exit angle.

flow exit angle: the angle between the fluid flow direction at the blade exit and the machine axial direction.

flow inlet angle: the angle between the fluid flow direction at the blade inlet and the machine axial direction.

hub: the portion of a turbomachine bounded by the inner surface of the flow annulus.

hub-tip ratio: same as hub-to-tip-radius ratio.

incidence angle: the flow inlet angle minus the blade inlet angle.

leading edge: the front, or nose, of the blade.

mean section: the blade section halfway between the hub and the tip.

pitch: the distance in the direction of rotation between corresponding points on adjacent blades.

rotor blade: a rotating blade.

solidity: the ratio of the chord to the spacing.

stagger angle: the angle between the chord line and the turbine axial direction (also known as the setting angle).

stator blade: a stationary blade.

suction surface: the convex surface of the blade. Along this surface, pressures are lowest.

tip: the outermost section of the blade or "vane."

trailing edge: the rear, or tail, of the blade.

Appendix 2

$$\frac{T_{02}}{T_{01}} = \left(\frac{P_{02}}{P_{01}}\right)^{\frac{1}{\eta_{c,\infty}}\frac{\gamma-1}{\gamma}}$$

$$\frac{T_0}{T} = 1\frac{C^2}{2\,c_p\,T} = 1 + \frac{\gamma-1}{2}M^2$$

$$\frac{T_0}{T} = \left(\frac{P_0}{P}\right)^{\frac{\gamma-1}{\gamma}}$$

$$\frac{m\sqrt{R\,T_0}}{P_0\,A} = \sqrt{\gamma}M\left(1 + \frac{\gamma-1}{2}M^2\right)^{-\frac{(\gamma+1)}{2\,(\gamma-1)}}$$

$$_D = 1 - \frac{V_2}{V_1} + \frac{\Delta C_w}{2\,V_1}.\frac{s}{c}$$

$$_P = \rho\,R\,T$$

$$_a = \sqrt{\gamma\,R\,T}$$

$$_A = \pi\,(r_t^2 - r_h^2)$$

$$M_{tip} = \frac{V_{tip}}{a}$$

$$M_{ax} = \frac{C_{ax}}{a}$$

$$_\emptyset = \frac{C}{U}$$

$$U_x = 2\,\pi\,r_x\,N$$

$$_\psi = \frac{\Delta h}{\frac{1}{2}U_m^2\,n}$$

Appendix 3

Disc geometry below for compressor type Hpc

Disc number 1

z: 0.5656 0.5656 0.5657 0.5658 0.5658 0.5659 0.5659 0.5660 0.5660 0.5661 0.5661 0.5661 0.5662 0.5662 0.5663 0.5663 0.5663 0.5664 0.5537 0.5537 0.5854 0.5854 0.5727 0.5727 0.5728 0.5728 0.5728 0.5729 0.5729 0.5730 0.5730 0.5731 0.5731 0.5732 0.5732 0.5733 0.5733 0.5734 0.5734 0.5734 0.5656

r: 0.0623 0.0940 0.0966 0.0993 0.1020 0.1046 0.1073 0.1100 0.1126 0.1153 0.1180 0.1207 0.1233 0.1260 0.1287 0.1313 0.1340 0.1367 0.1491 0.1615 0.1615 0.1491 0.1367 0.1340 0.1313 0.1287 0.1260 0.1233 0.1207 0.1180 0.1153 0.1126 0.1100 0.1073 0.1046 0.1020 0.0993 0.0966 0.0940 0.0623 0.0623

Tangential stresses: 0.520720E+09 0.354699E+09 0.256957E+09 0.229851E+09 0.204907E+09

Radial stresses: 0.000000E+00 0.100057E+09 0.955025E+08 0.662133E+08 0.398223E+08

Disc geometry below for compressor type Hpc

Disc number 2

z: 0.6457 0.6457 0.6458 0.6459 0.6459 0.6460 0.6461 0.6461 0.6462 0.6462 0.6463 0.6463 0.6464 0.6464 0.6465 0.6465 0.6465 0.6466 0.6360 0.6360 0.6625 0.6625 0.6519 0.6519 0.6519 0.6520 0.6520 0.6521 0.6521 0.6522 0.6522 0.6523 0.6523 0.6524 0.6524 0.6525 0.6525 0.6526 0.6527 0.6527 0.6457

r: 0.0644 0.0908 0.0941 0.0973 0.1005 0.1037 0.1069 0.1101 0.1134 0.1166 0.1198 0.1230 0.1262 0.1294 0.1326 0.1359 0.1391 0.1423 0.1553 0.1683 0.1683 0.1553 0.1423 0.1391 0.1359 0.1326 0.1294 0.1262 0.1230 0.1198 0.1166 0.1134 0.1101 0.1069 0.1037 0.1005 0.0973 0.0941 0.0908 0.0644 0.0644

Tangential stresses: 0.520720E+09 0.374749E+09 0.252871E+09 0.224636E+09 0.198204E+09

Radial stresses: 0.000000E+00 0.911542E+08 0.896558E+08 0.579103E+08 0.282742E+08

Disc geometry below for compressor type Hpc

Disc number 3

z: 0.7131 0.7131 0.7132 0.7133 0.7134 0.7134 0.7135 0.7136 0.7136 0.7137 0.7137 0.7138 0.7138 0.7139 0.7139 0.7139 0.7140 0.7140 0.7048 0.7048 0.7278 0.7278 0.7186 0.7187 0.7187 0.7187 0.7188 0.7188 0.7189 0.7189 0.7190 0.7190 0.7191 0.7191 0.7192 0.7193 0.7194 0.7194 0.7195 0.7195 0.7131

r: 0.0658 0.0888 0.0926 0.0964 0.1003 0.1041 0.1079 0.1117 0.1155 0.1194 0.1232 0.1270 0.1308 0.1346 0.1385 0.1423 0.1461 0.1499 0.1614 0.1730 0.1730 0.1614 0.1499 0.1461 0.1423 0.1385 0.1346 0.1308 0.1270 0.1232 0.1194 0.1155 0.1117 0.1079 0.1041 0.1003 0.0964 0.0926 0.0888 0.0658 0.0658

Tangential stresses: 0.520720E+09 0.389379E+09 0.242509E+09 0.217777E+09 0.194209E+09

Radial stresses: 0.000000E+00 0.838773E+08 0.787239E+08 0.494585E+08 0.216790E+08

Disc geometry below for compressor type Hpc

Disc number 4

z: 0.7715 0.7715 0.7716 0.7718 0.7719 0.7720 0.7721 0.7722 0.7723 0.7724 0.7725 0.7726 0.7726 0.7727 0.7728 0.7728 0.7729 0.7729 0.7647 0.7647 0.7854 0.7854 0.7771 0.7771 0.7772 0.7773 0.7773 0.7774 0.7775 0.7775 0.7776 0.7777 0.7778 0.7779 0.7780 0.7781 0.7783 0.7784 0.7786 0.7786 0.7715

r: 0.0668 0.0875 0.0917 0.0960 0.1002 0.1045 0.1087 0.1130 0.1173 0.1215 0.1258 0.1300 0.1343 0.1385 0.1428 0.1470 0.1513 0.1556 0.1659 0.1763 0.1763 0.1659 0.1556 0.1513 0.1470 0.1428 0.1385 0.1343 0.1300 0.1258 0.1215 0.1173 0.1130 0.1087 0.1045 0.1002 0.0960 0.0917 0.0875 0.0668 0.0668

Tangential stresses: 0.520720E+09 0.399784E+09 0.243909E+09 0.221971E+09 0.201062E+09

Radial stresses: 0.000000E+00 0.783147E+08 0.880354E+08 0.593668E+08 0.329988E+08

Disc geometry below for compressor type Hpc

Disc number 5

z: 0.8248 0.8248 0.8249 0.8251 0.8252 0.8253 0.8254 0.8255 0.8256 0.8257 0.8258 0.8258 0.8259 0.8260 0.8260 0.8261 0.8262 0.8262 0.8185 0.8185 0.8378 0.8378 0.8301 0.8301 0.8302 0.8302 0.8303 0.8304 0.8304 0.8305 0.8306 0.8307 0.8308 0.8309 0.8310 0.8311 0.8312 0.8314 0.8315 0.8315 0.8248

r: 0.0675 0.0867 0.0913 0.0958 0.1004 0.1049 0.1094 0.1140 0.1185 0.1231 0.1276 0.1322 0.1367 0.1412 0.1458 0.1503 0.1549 0.1594 0.1690 0.1787 0.1787 0.1690 0.1594 0.1549 0.1503 0.1458 0.1412 0.1367 0.1322 0.1276 0.1231 0.1185 0.1140 0.1094 0.1049 0.1004 0.0958 0.0913 0.0867 0.0675 0.0675

Tangential stresses: 0.520720E+09 0.406755E+09 0.238314E+09 0.217967E+09 0.198424E+09

Radial stresses: 0.000000E+00 0.743760E+08 0.805416E+08 0.536047E+08 0.285151E+08

Appendix 4

Disk 1

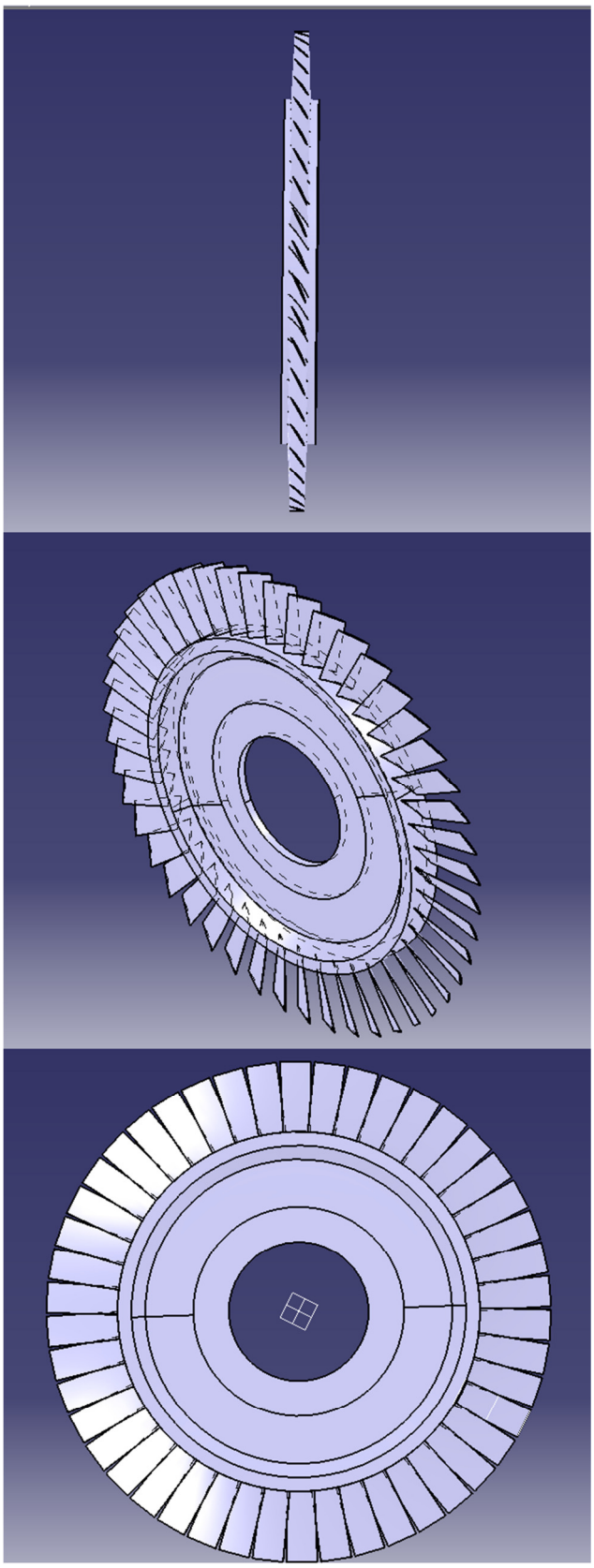

Disk 2

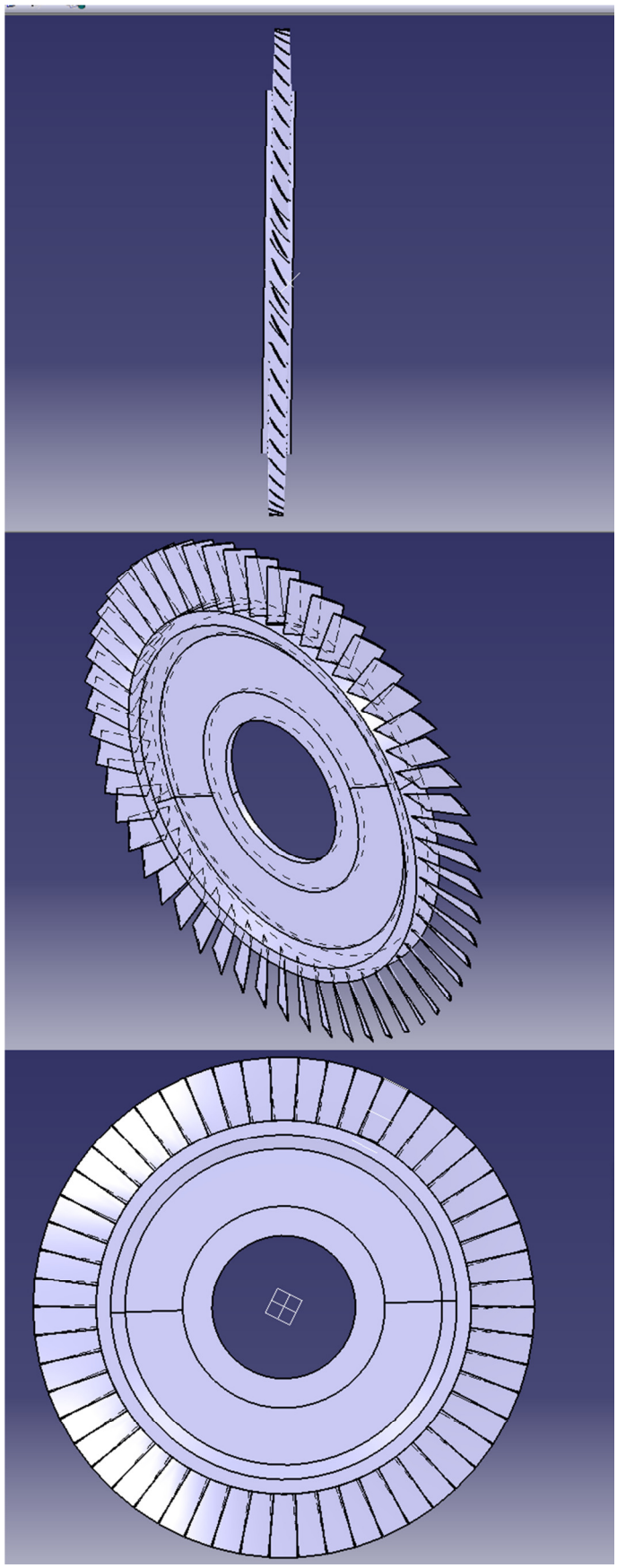

Disk 3

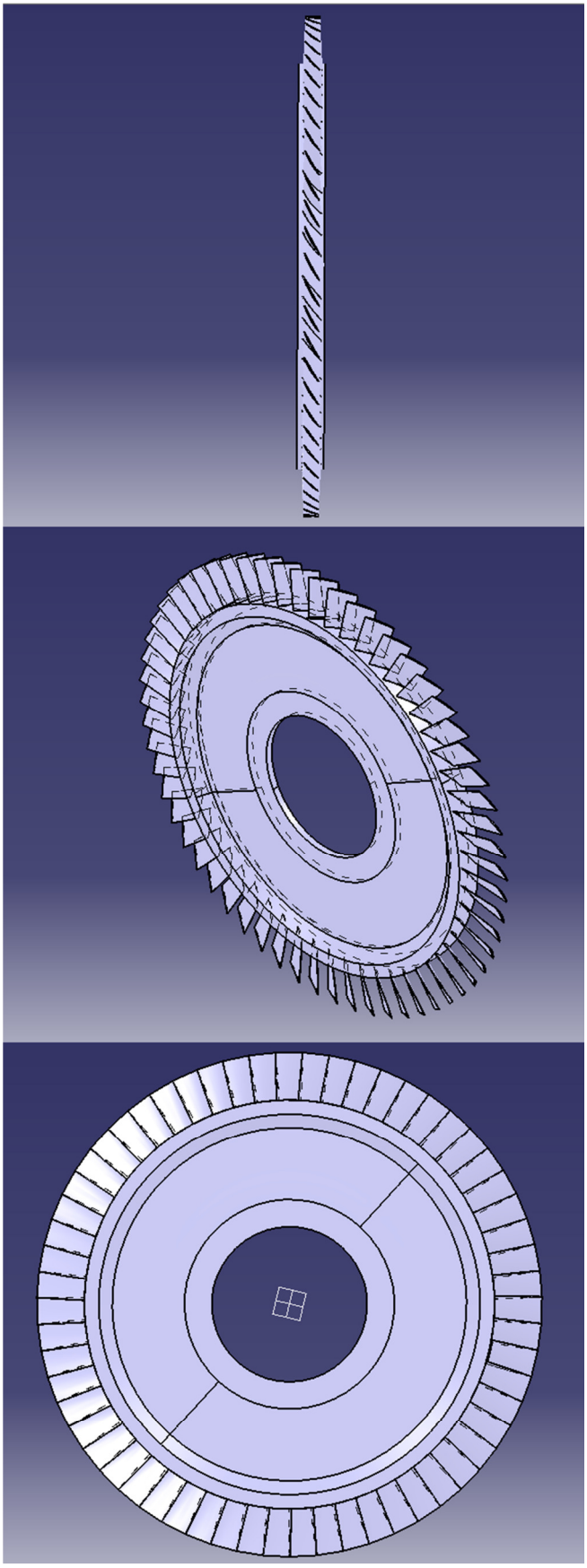

Disk 4

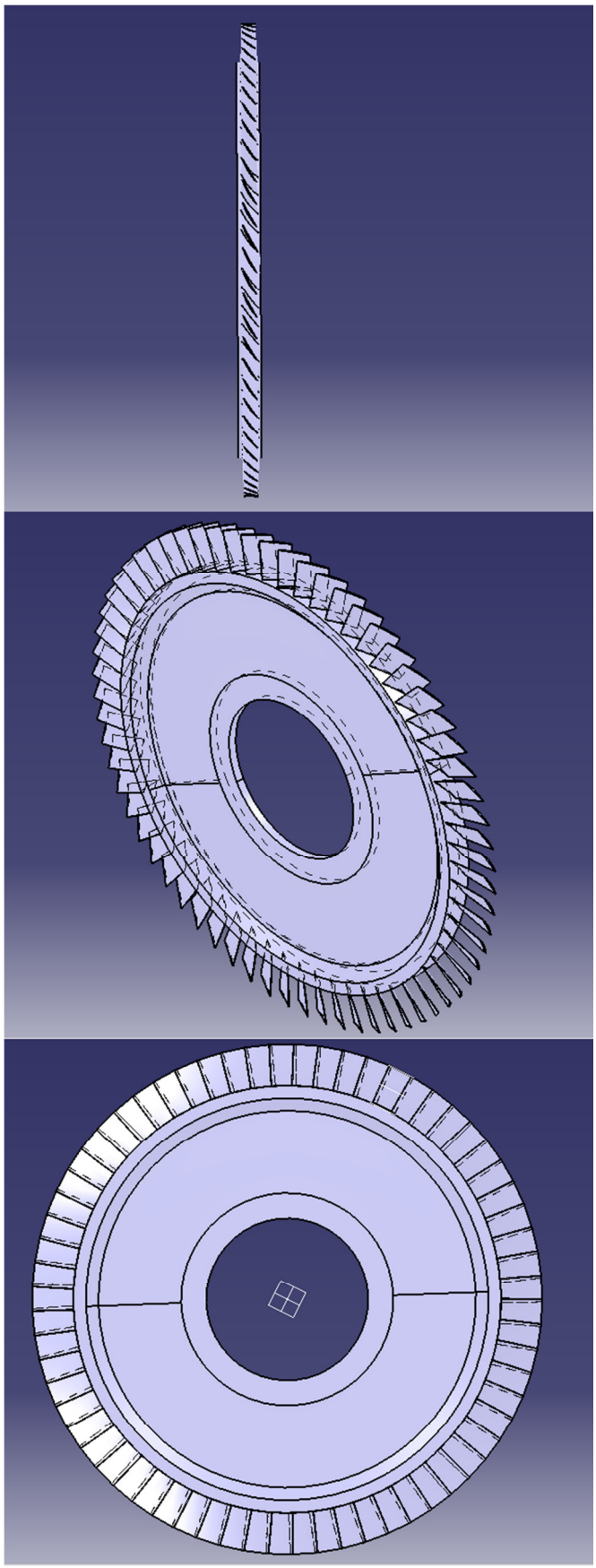

Disk 5

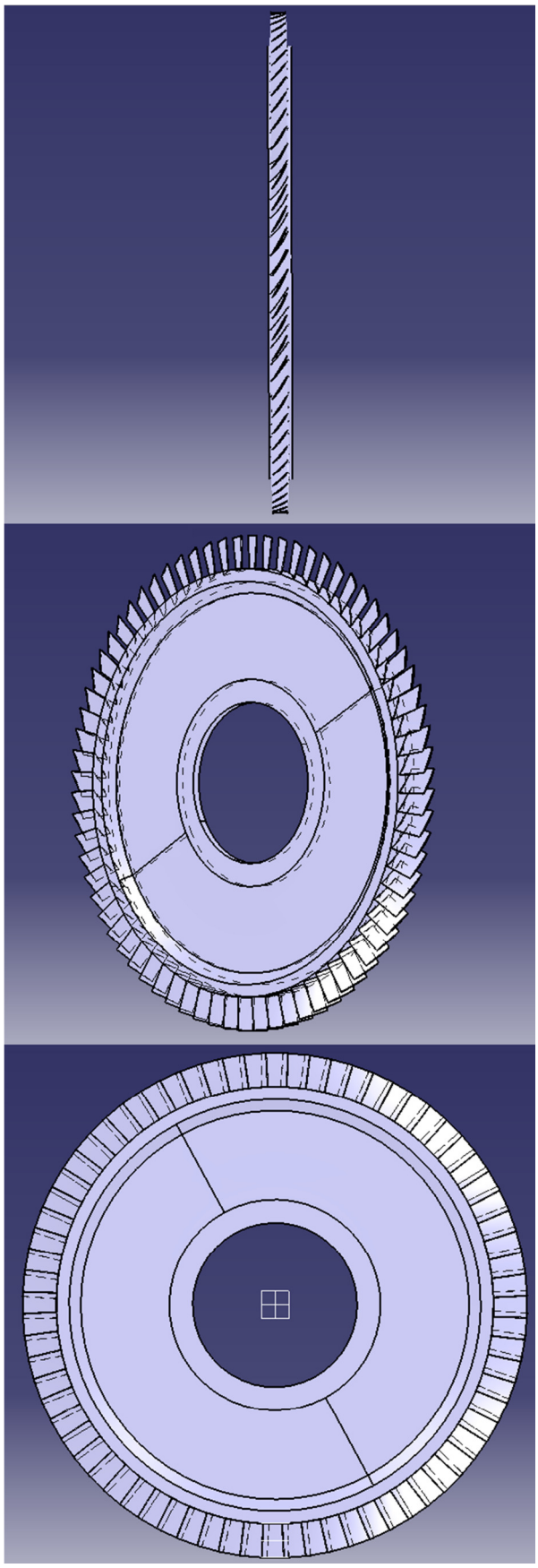

Appendix 5

Disk 1

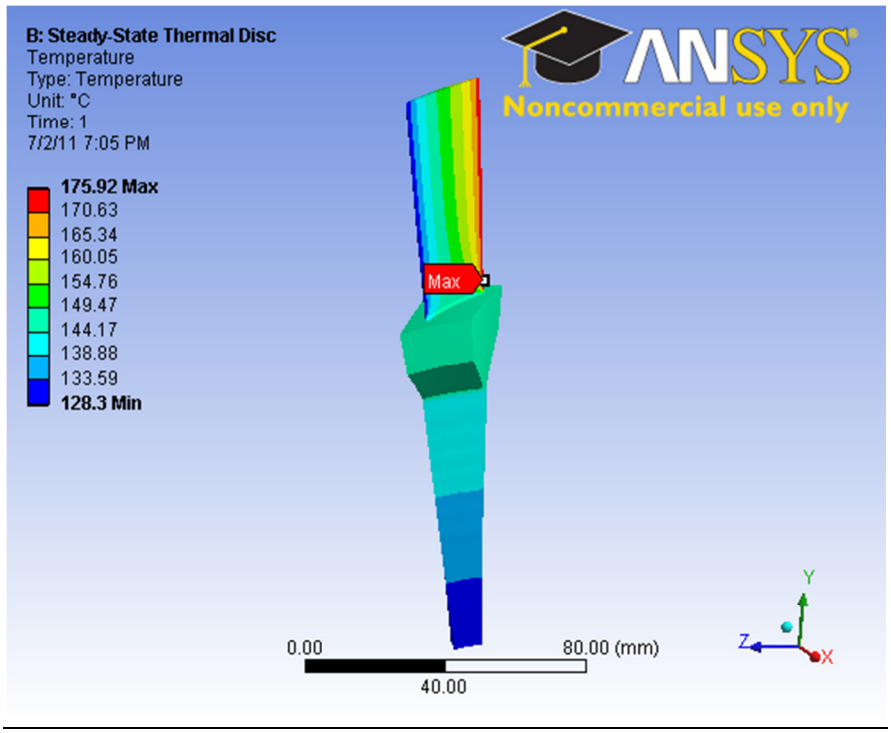

Disk 2

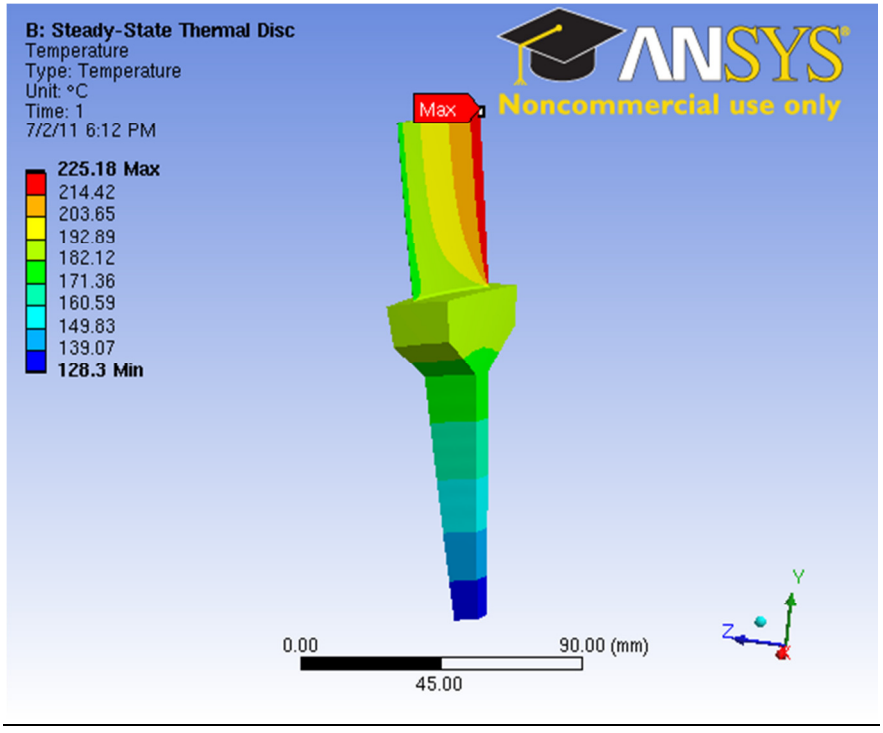

Disk 3

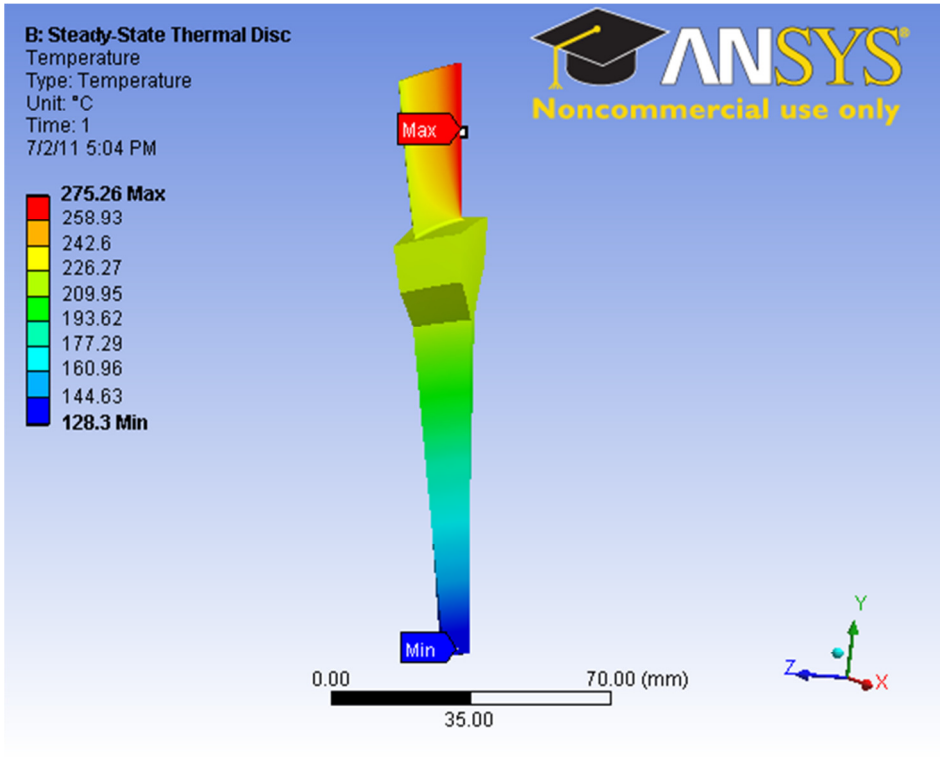
B: Steady-State Thermal Disc
Temperature
Type: Temperature
Unit: °C
Time: 1
7/2/11 5:04 PM
275.26 Max
258.93
242.6
226.27
209.95
193.62
177.29
160.96
144.63
128.3 Min
Max
Min
ANSYS
Noncommercial use only
0.00
70.00 (mm)
35.00
Y
Z
X

Disk 4

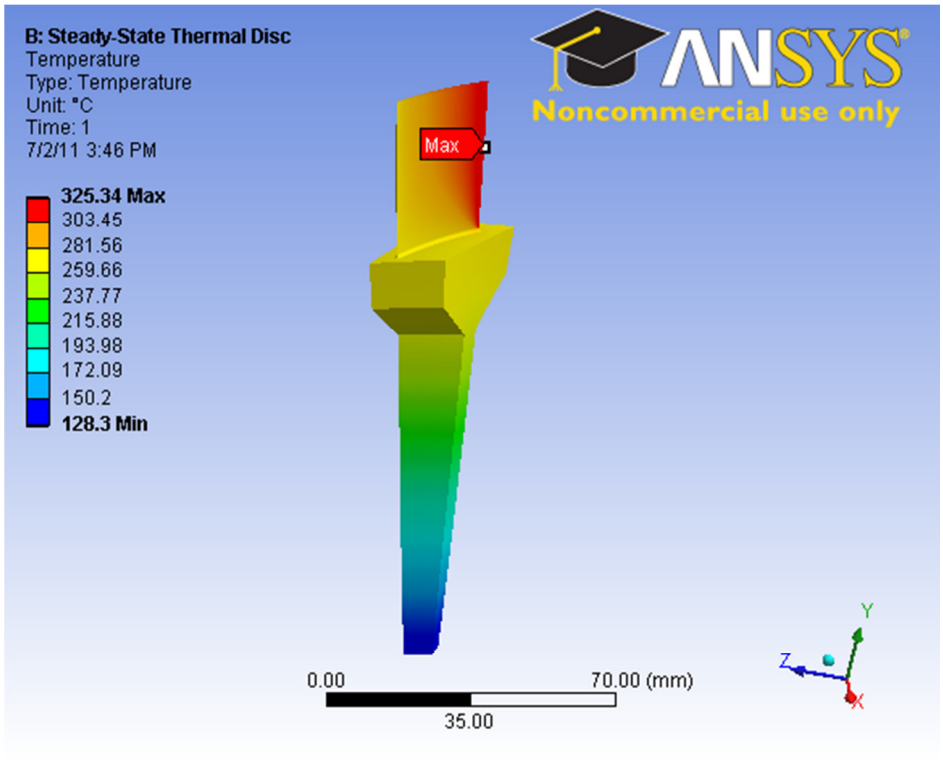
B: Steady-State Thermal Disc
Temperature
Type: Temperature
Unit: °C
Time: 1
7/2/11 3:46 PM
325.34 Max
303.45
281.56
259.66
237.77
215.88
193.98
172.09
150.2
128.3 Min
Max
ANSYS
Noncommercial use only
0.00
70.00 (mm)
35.00
Y
Z
X

Disk 5

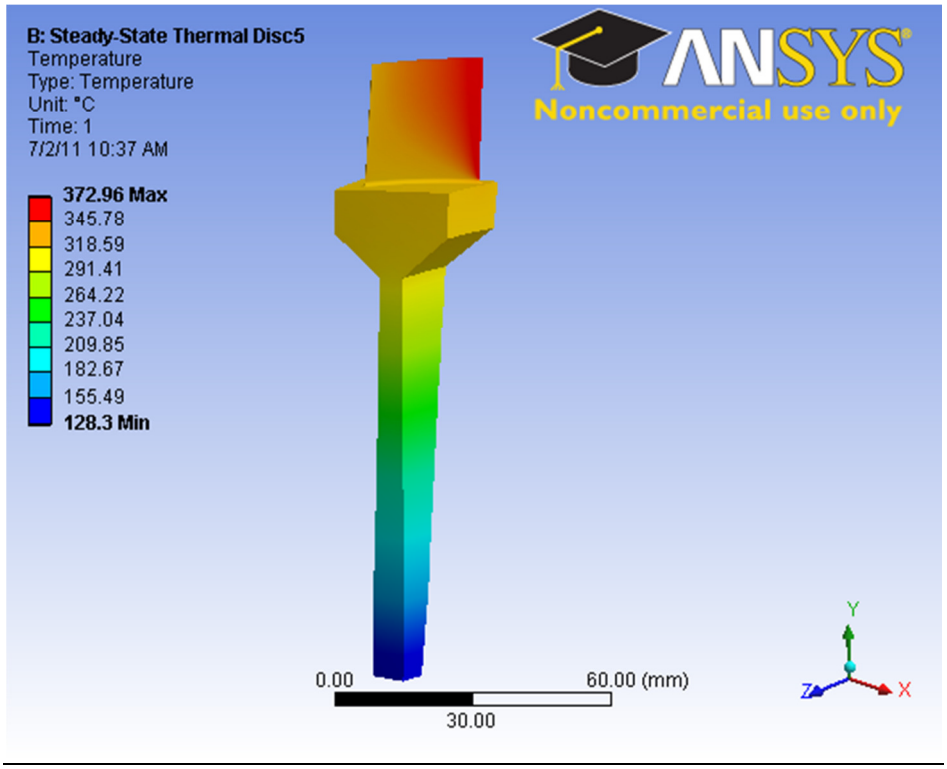
B: Steady-State Thermal Disc5
Temperature
Type: Temperature
Unit: °C
Time: 1
7/2/11 10:37 AM
372.96 Max
345.78
318.59
291.41
264.22
237.04
209.85
182.67
155.49
128.3 Min
ANSYS
Noncommercial use only
0.00
60.00 (mm)
30.00
Y
Z
X

Appendix 6

Disc 1

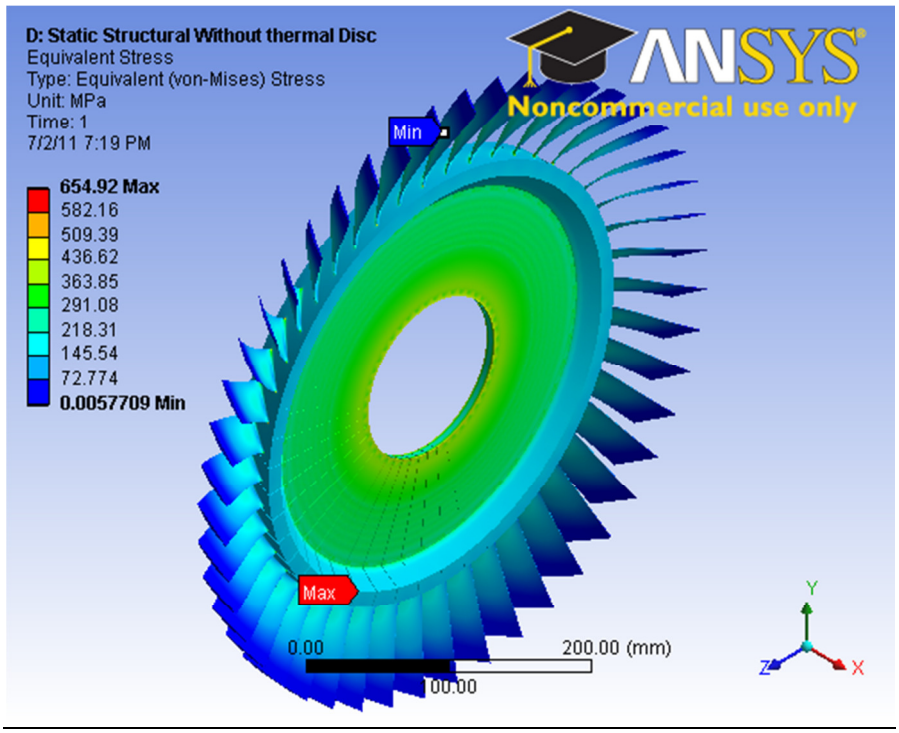

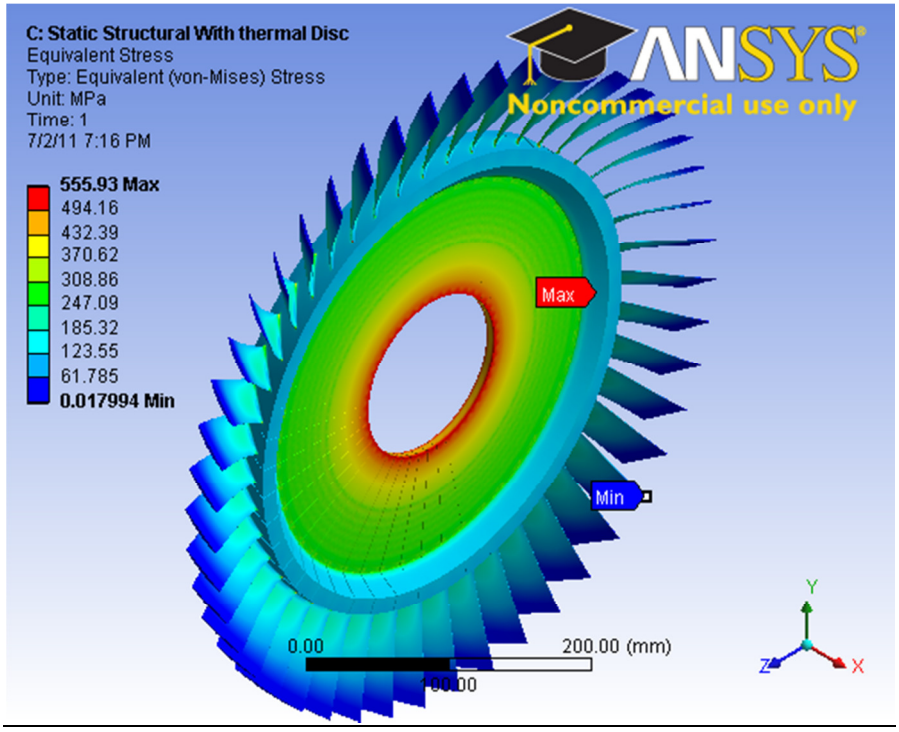

Disc 2

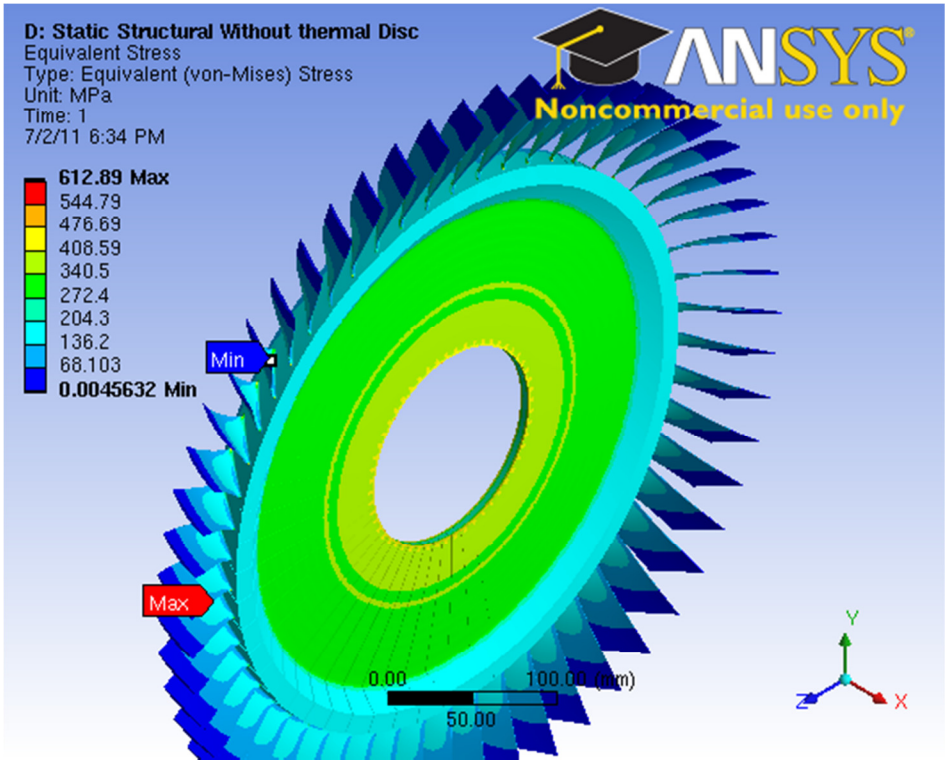
D: Static Structural Without thermal Disc
Equivalent Stress
Type: Equivalent (von-Mises) Stress
Unit: MPa
Time: 1
7/2/11 6:34 PM
612.89 Max
544.79
476.69
408.59
340.5
272.4
204.3
136.2
68.103
0.0045632 Min
Min
Max
0.00
100.00 (mm)
50.00
Y
Z
X
ANSYS
Noncommercial use only

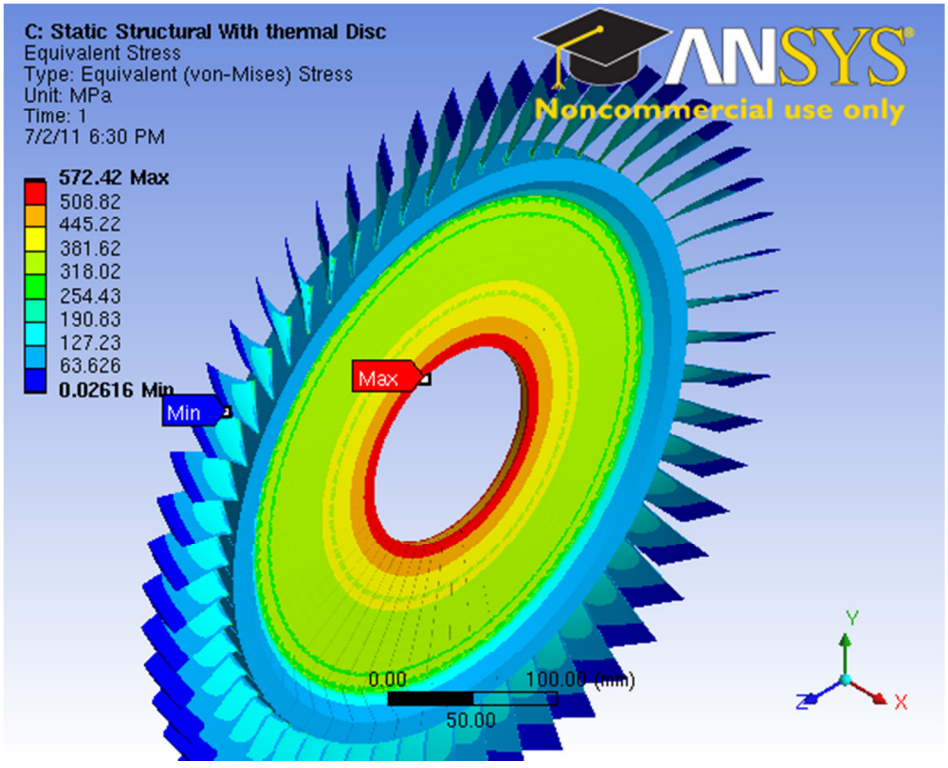
C: Static Structural With thermal Disc
Equivalent Stress
Type: Equivalent (von-Mises) Stress
Unit: MPa
Time: 1
7/2/11 6:30 PM
572.42 Max
508.82
445.22
381.62
318.02
254.43
190.83
127.23
63.626
0.02616 Min
Max
Min
0.00
100.00 (mm)
50.00
Y
Z
X
ANSYS
Noncommercial use only

Disc 3

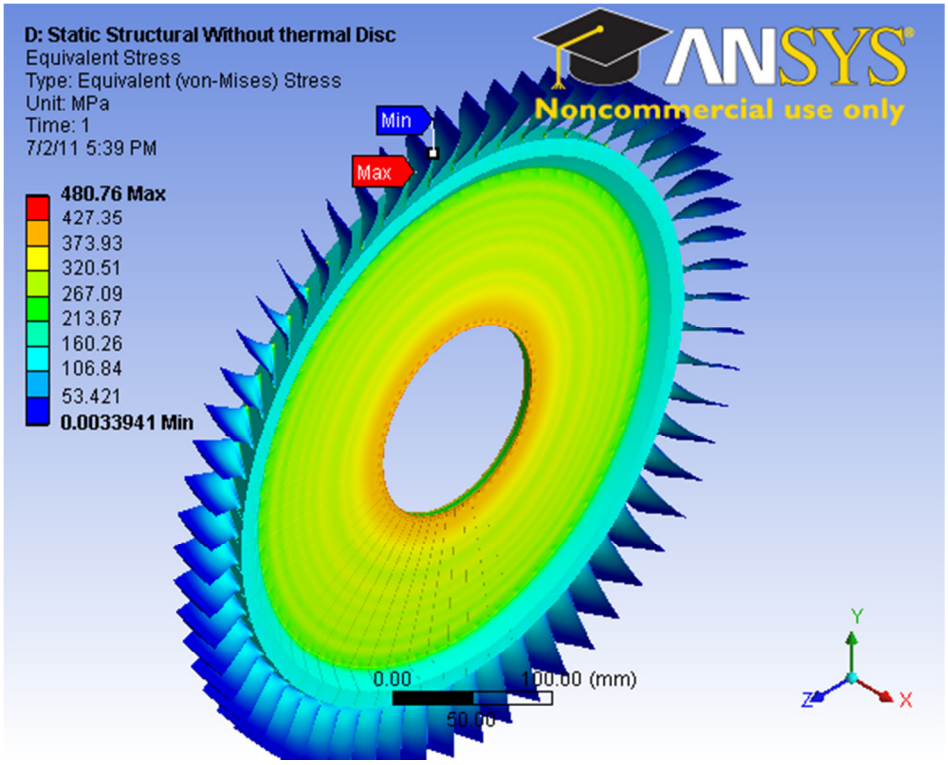
D: Static Structural Without thermal Disc
Equivalent Stress
Type: Equivalent (von-Mises) Stress
Unit: MPa
Time: 1
7/2/11 5:39 PM
480.76 Max
427.35
373.93
320.51
267.09
213.67
160.26
106.84
53.421
0.0033941 Min
Min
Max
ANSYS
Noncommercial use only
0.00
100.00 (mm)
50.00
Y
Z
X

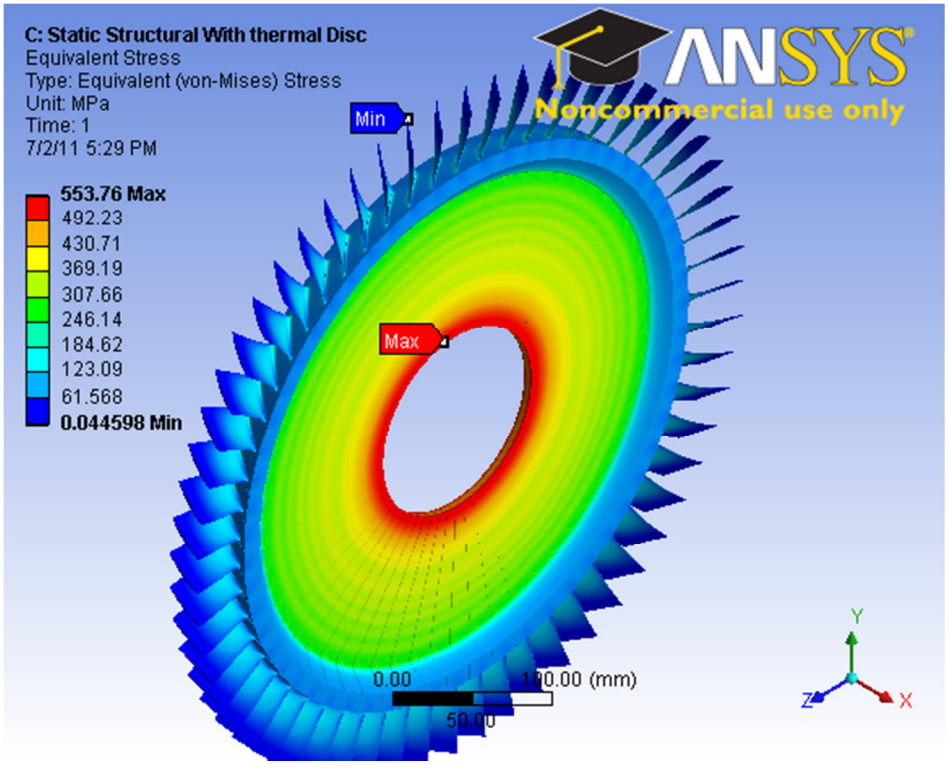
C: Static Structural With thermal Disc
Equivalent Stress
Type: Equivalent (von-Mises) Stress
Unit: MPa
Time: 1
7/2/11 5:29 PM
553.76 Max
492.23
430.71
369.19
307.66
246.14
184.62
123.09
61.568
0.044598 Min
Min
Max
ANSYS
Noncommercial use only
0.00
100.00 (mm)
50.00
Y
Z
X

Disc 4

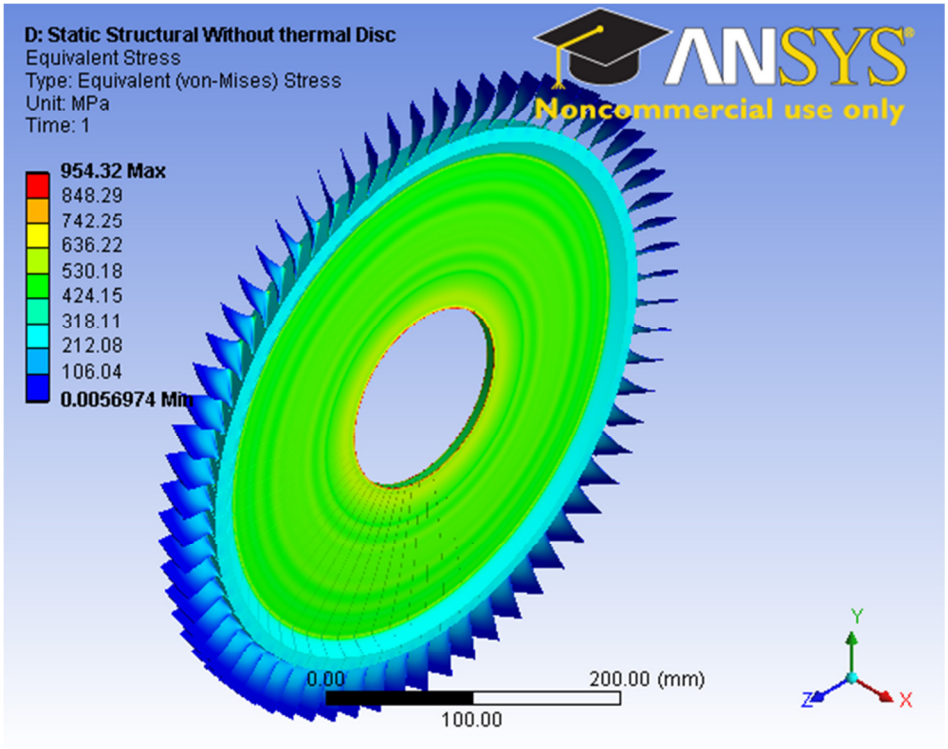
D: Static Structural Without thermal Disc
Equivalent Stress
Type: Equivalent (von-Mises) Stress
Unit: MPa
Time: 1
954.32 Max
848.29
742.25
636.22
530.18
424.15
318.11
212.08
106.04
0.0056974 Min
ANSYS
Noncommercial use only
0.00
200.00 (mm)
100.00
Y
Z
X

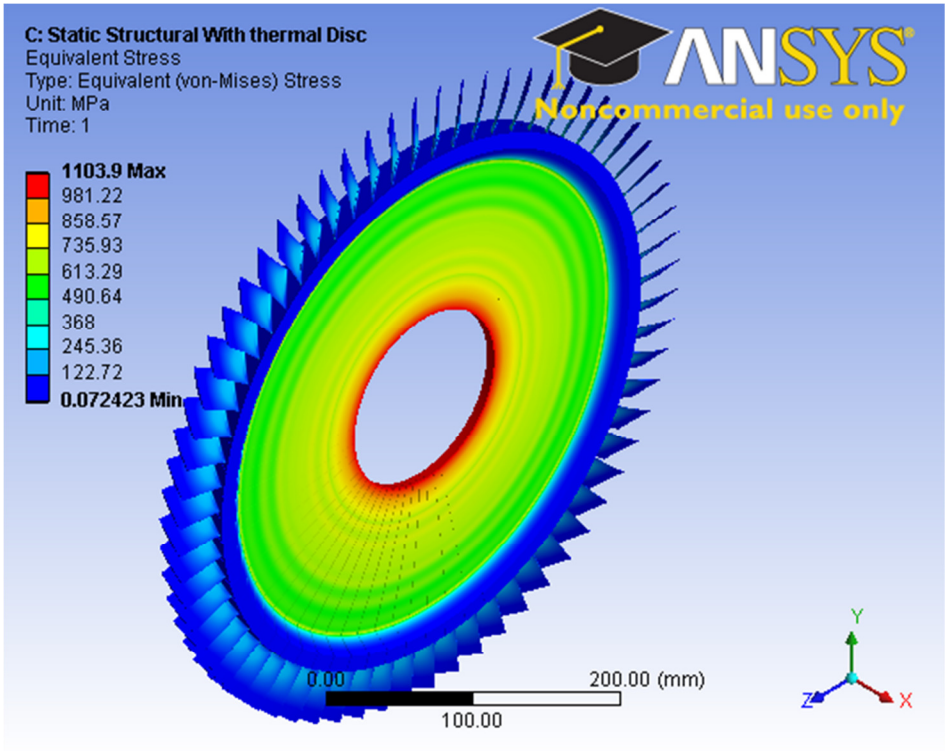
C: Static Structural With thermal Disc
Equivalent Stress
Type: Equivalent (von-Mises) Stress
Unit: MPa
Time: 1
1103.9 Max
981.22
858.57
735.93
613.29
490.64
368
245.36
122.72
0.072423 Min
ANSYS
Noncommercial use only
0.00
200.00 (mm)
100.00
Y
Z
X

Disc 5

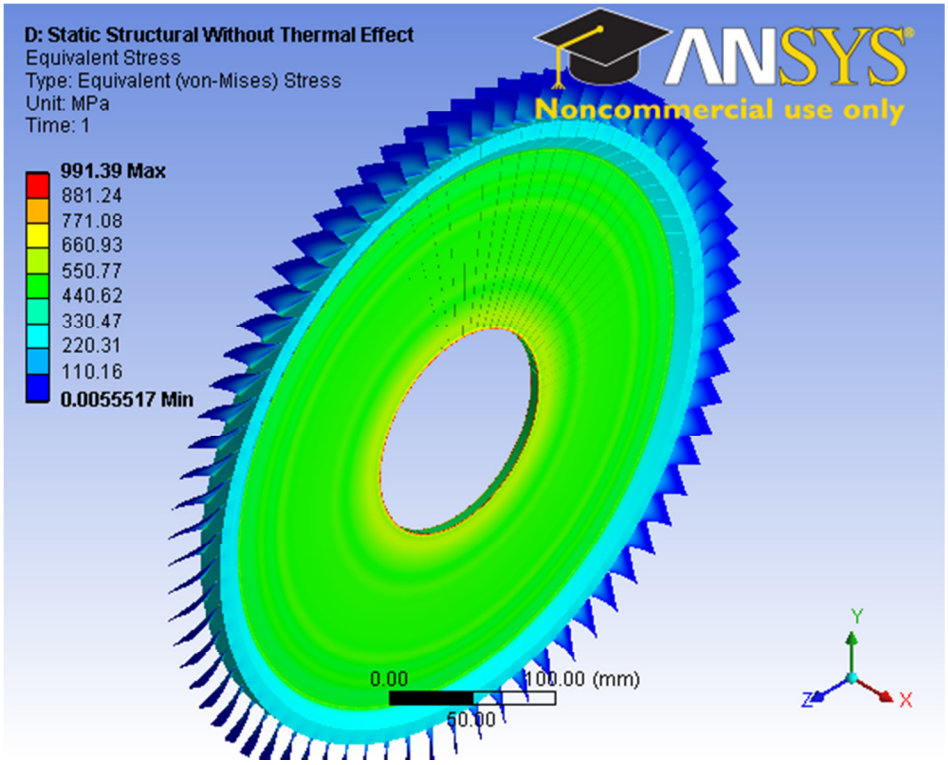
D: Static Structural Without Thermal Effect
Equivalent Stress
Type: Equivalent (von-Mises) Stress
Unit: MPa
Time: 1
991.39 Max
881.24
771.08
660.93
550.77
440.62
330.47
220.31
110.16
0.0055517 Min
ANSYS
Noncommercial use only
0.00
100.00 (mm)
50.00
Y
Z
X

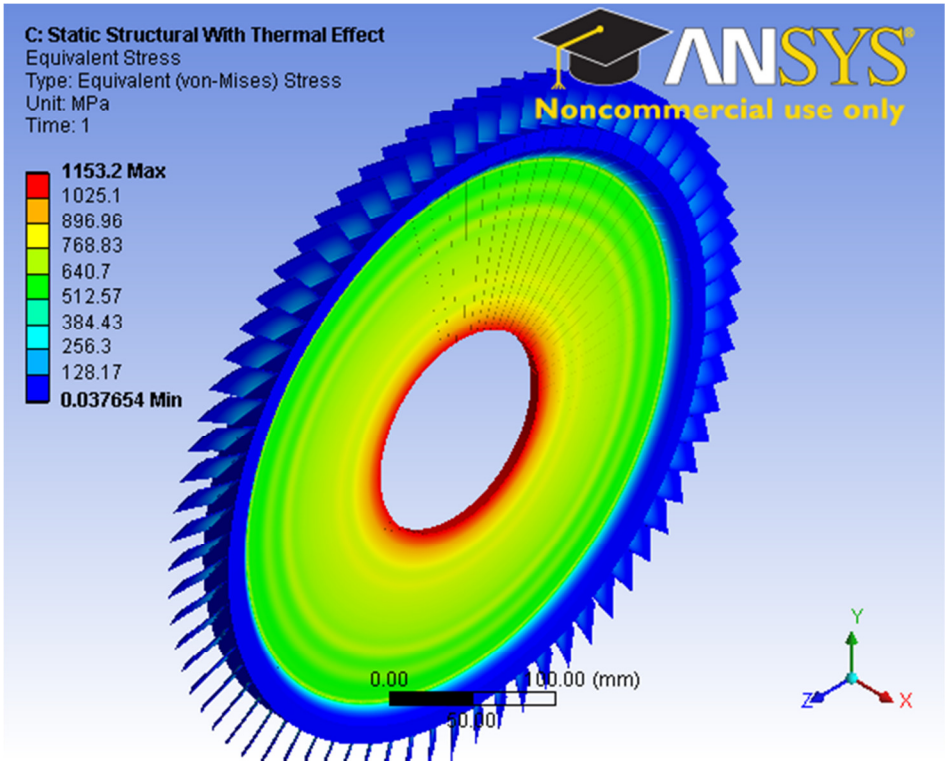
C: Static Structural With Thermal Effect
Equivalent Stress
Type: Equivalent (von-Mises) Stress
Unit: MPa
Time: 1
1153.2 Max
1025.1
896.96
768.83
640.7
512.57
384.43
256.3
128.17
0.037654 Min
ANSYS
Noncommercial use only
0.00
100.00 (mm)
50.00
Y
Z
X

Appendix 7

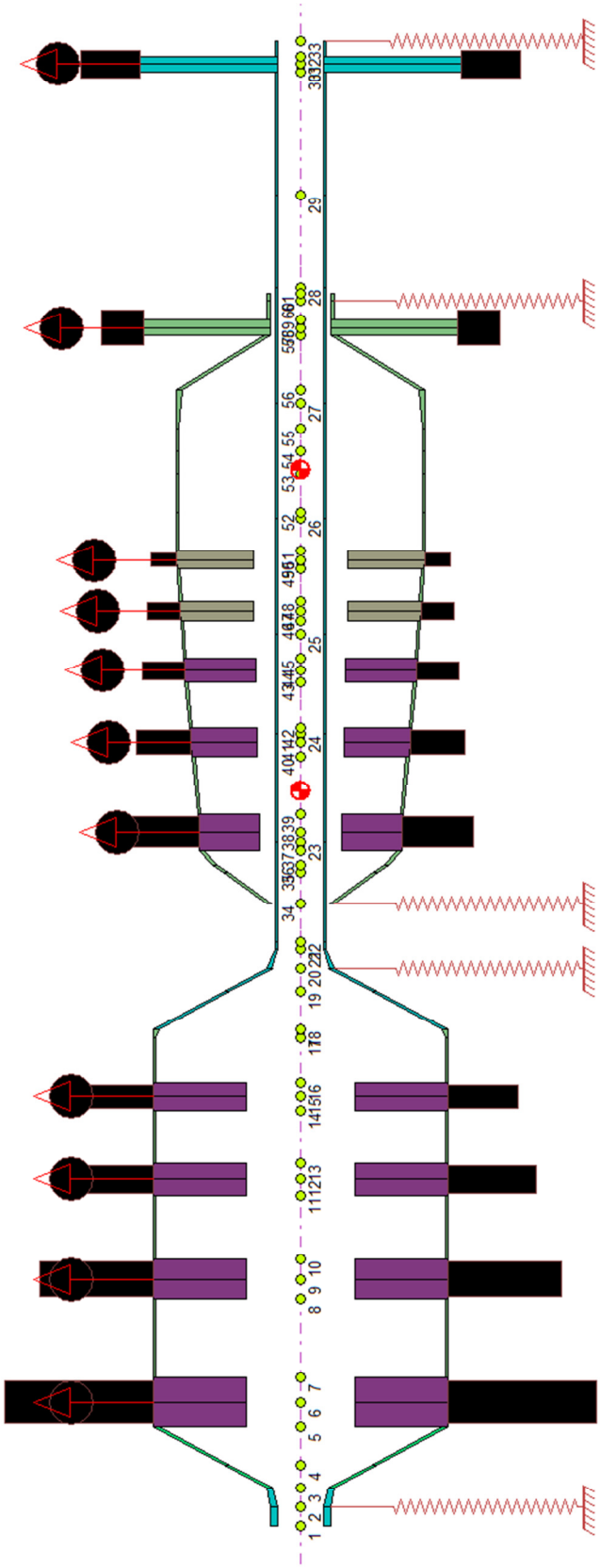

Appendix 8

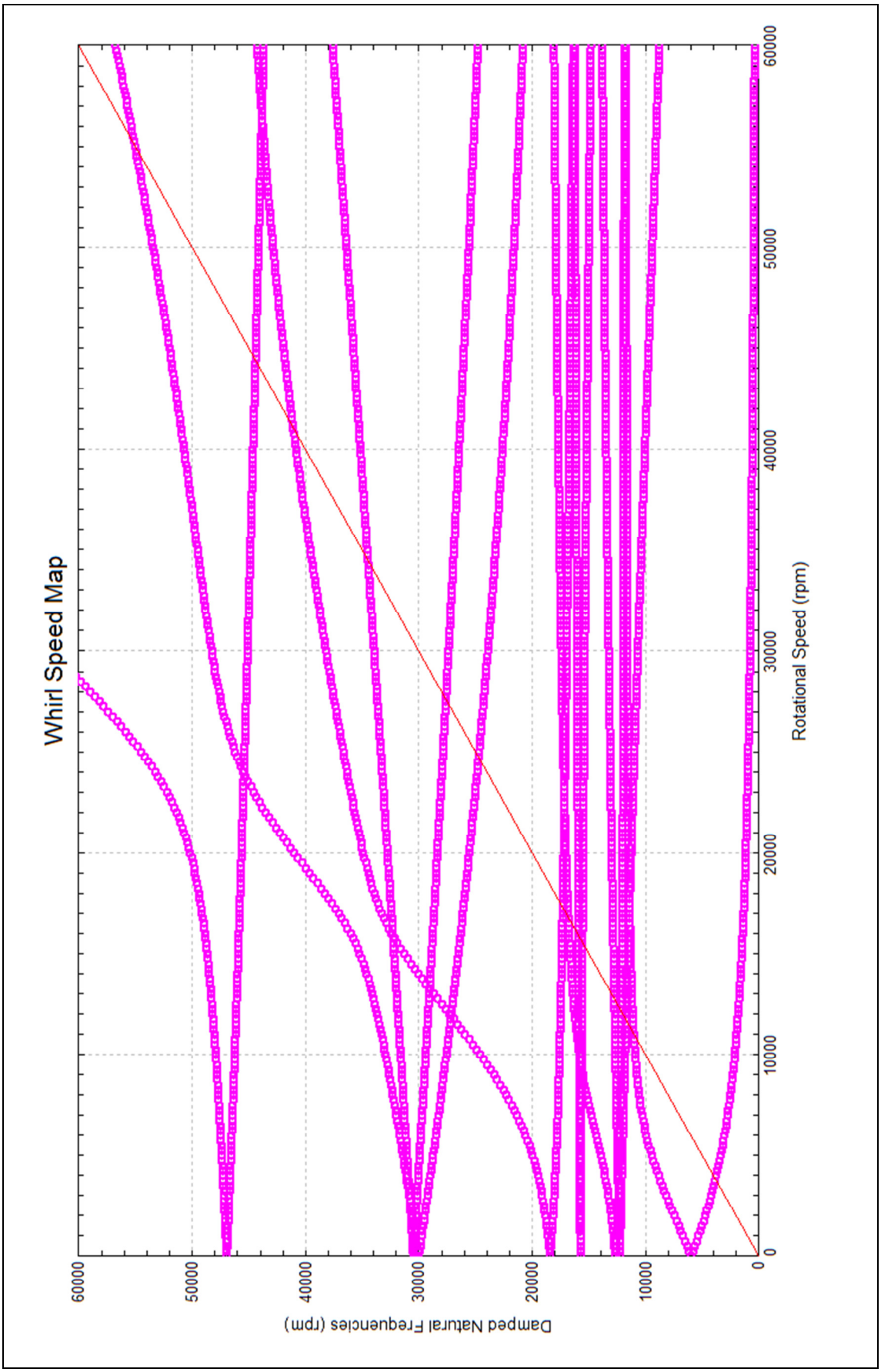
Whirl Speed Map
Rotational Speed (rpm)
Damped Natural Frequencies (rpm)
0
10000
20000
30000
40000
50000
60000

Appendix 9

1st critical speed for LP rotor

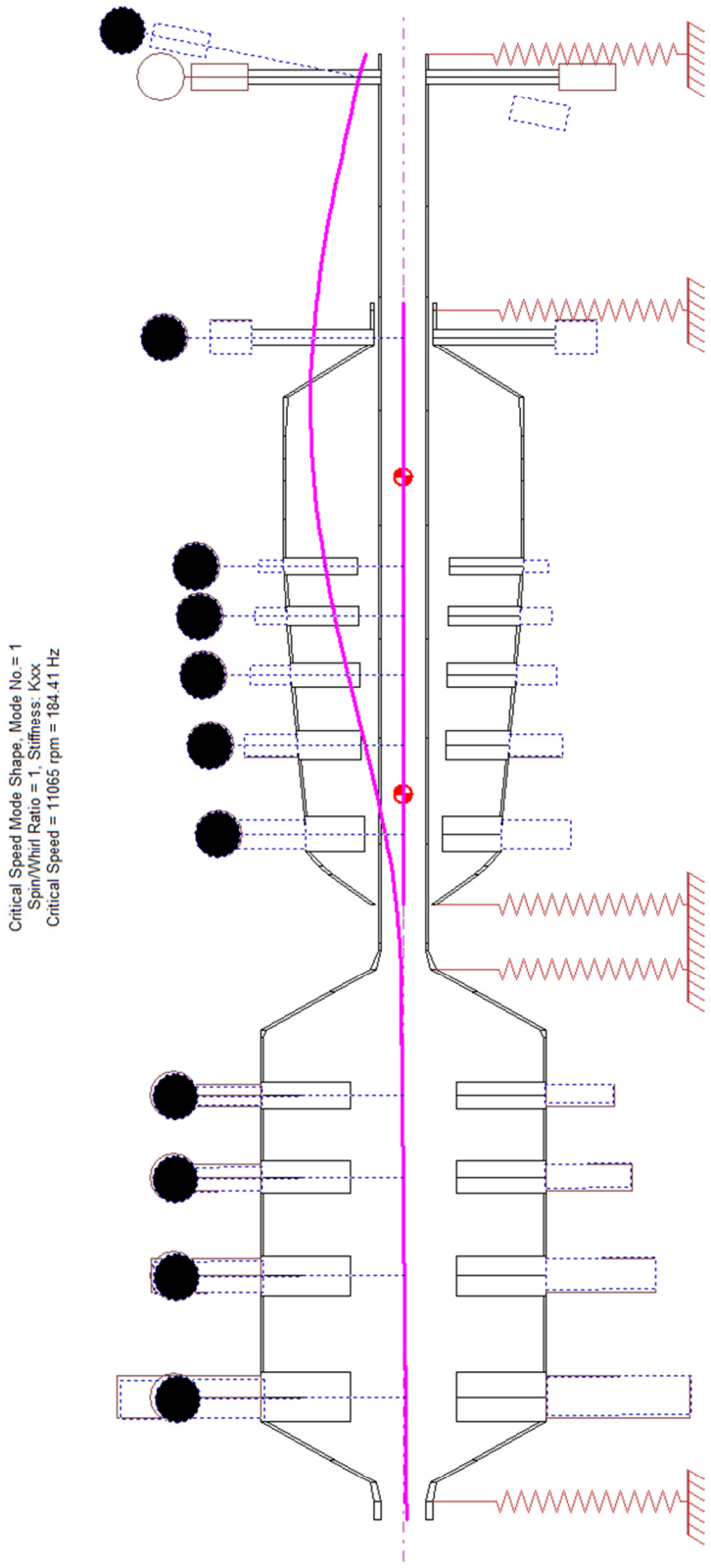

2nd critical speed for LP rotor

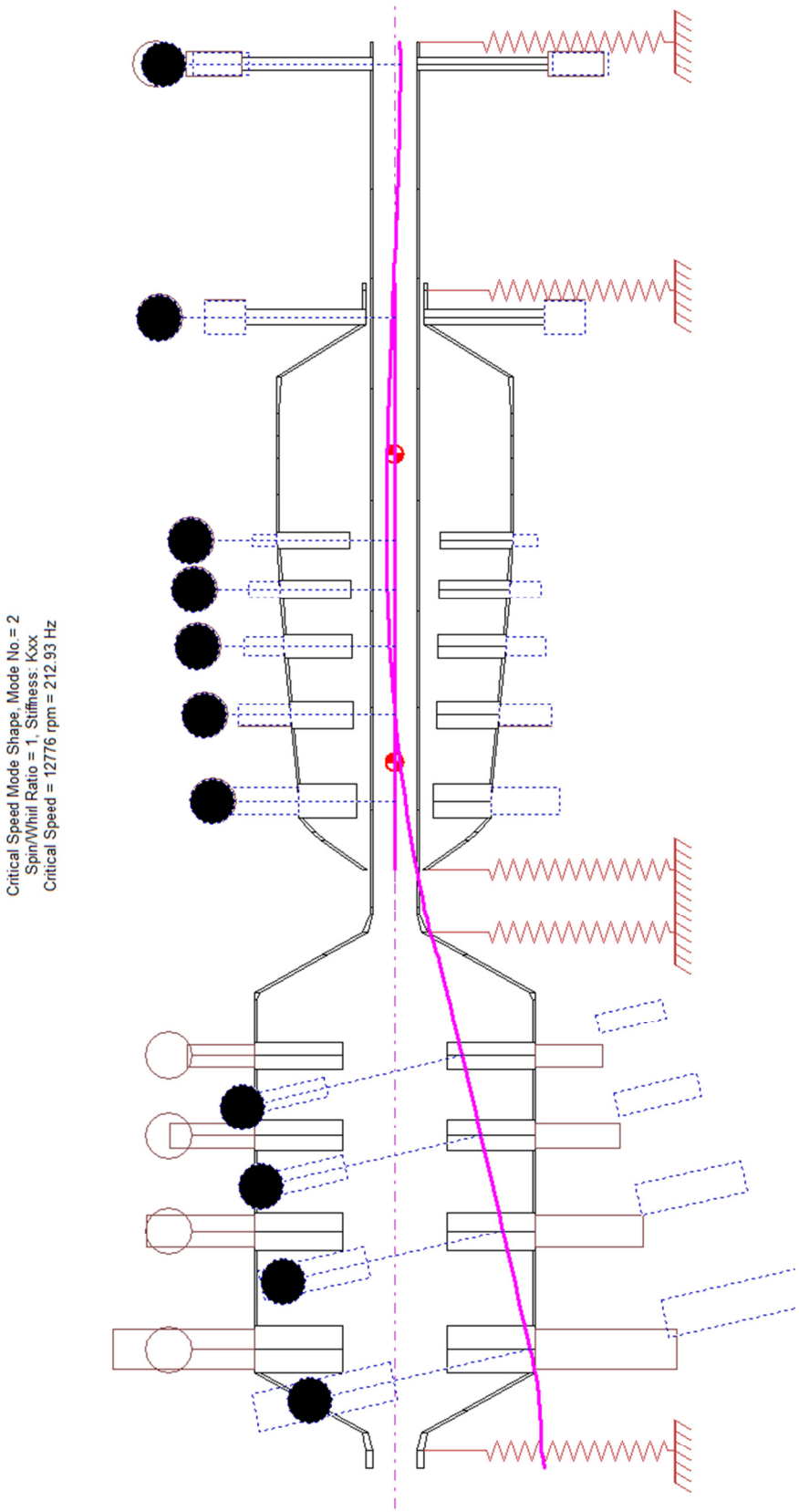

3rd critical speed for HP rotor

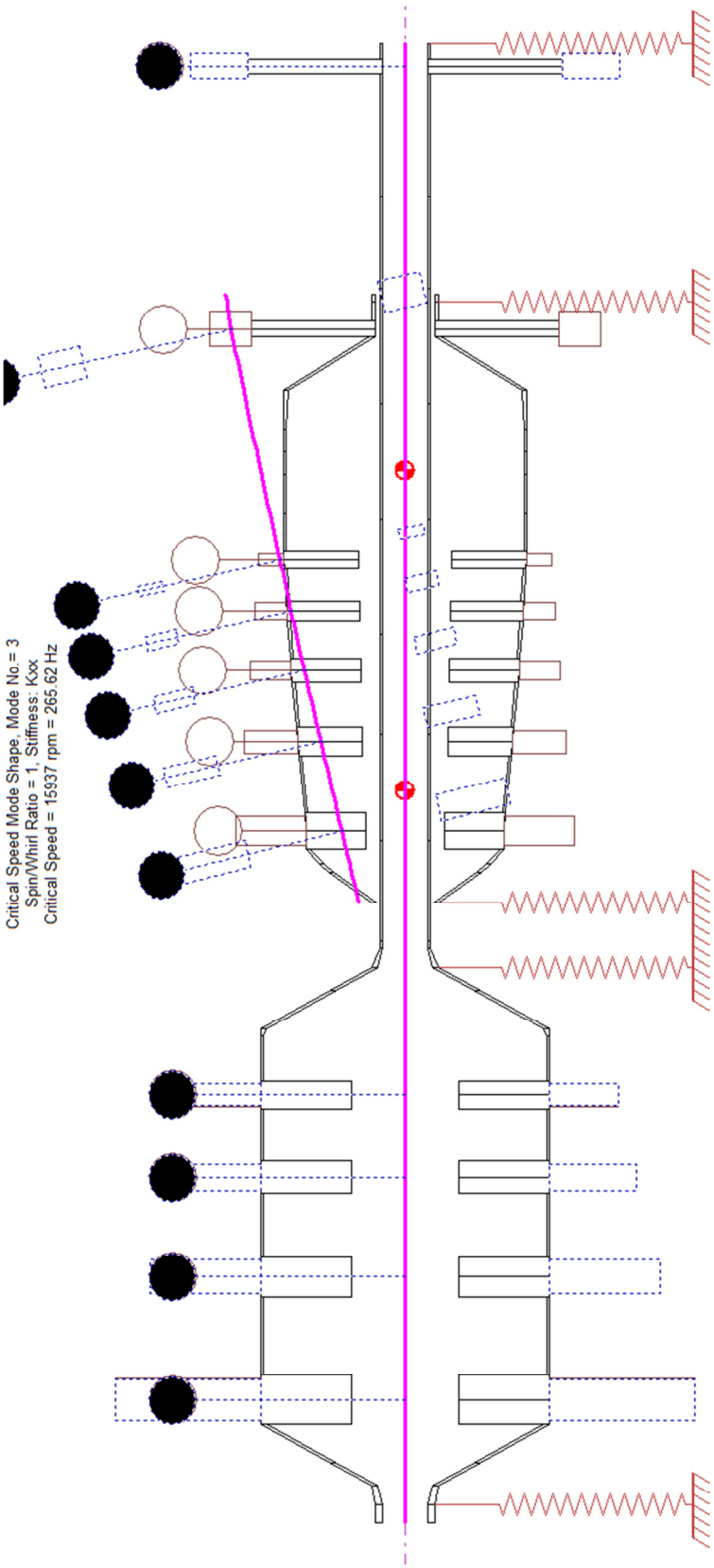

4th critical speed for LP rotor

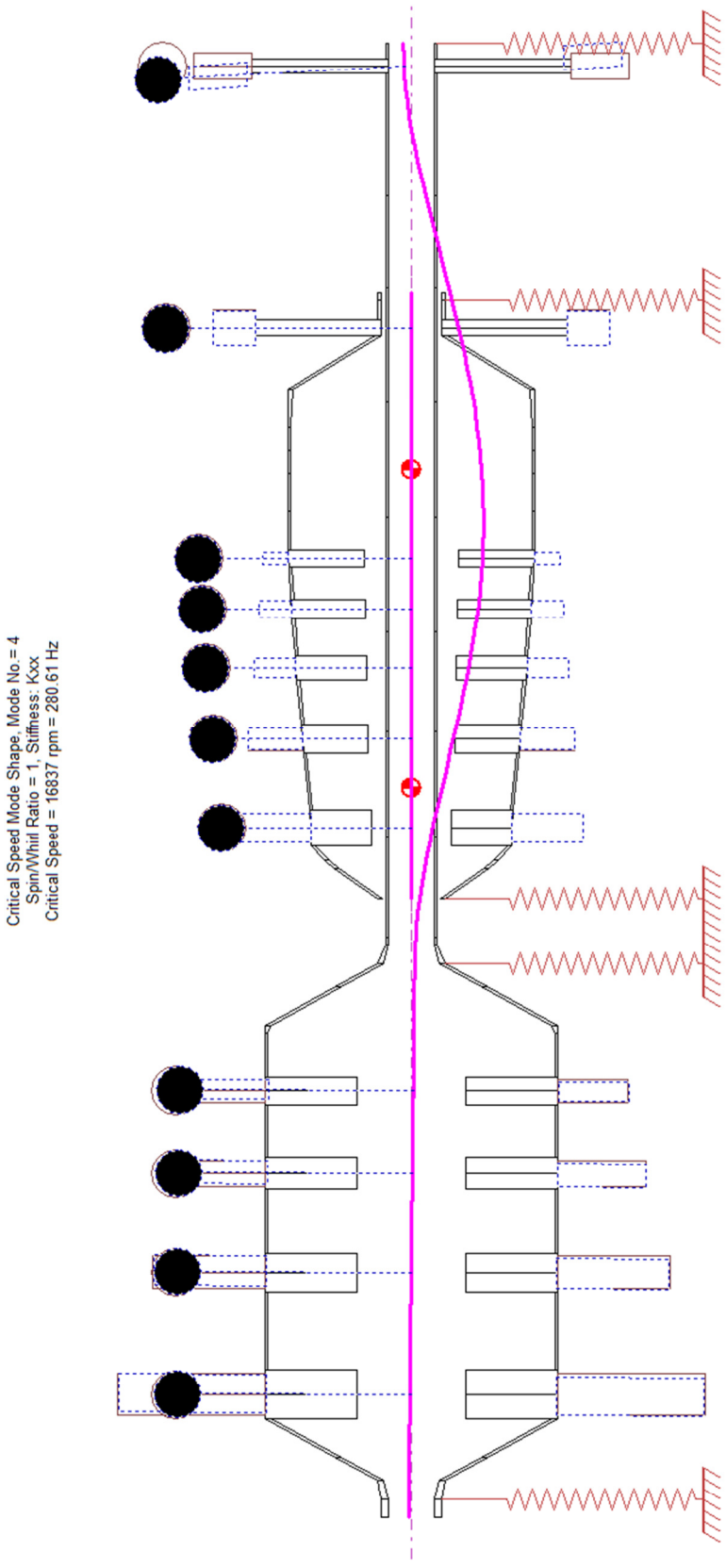

5th critical speed for HP rotor

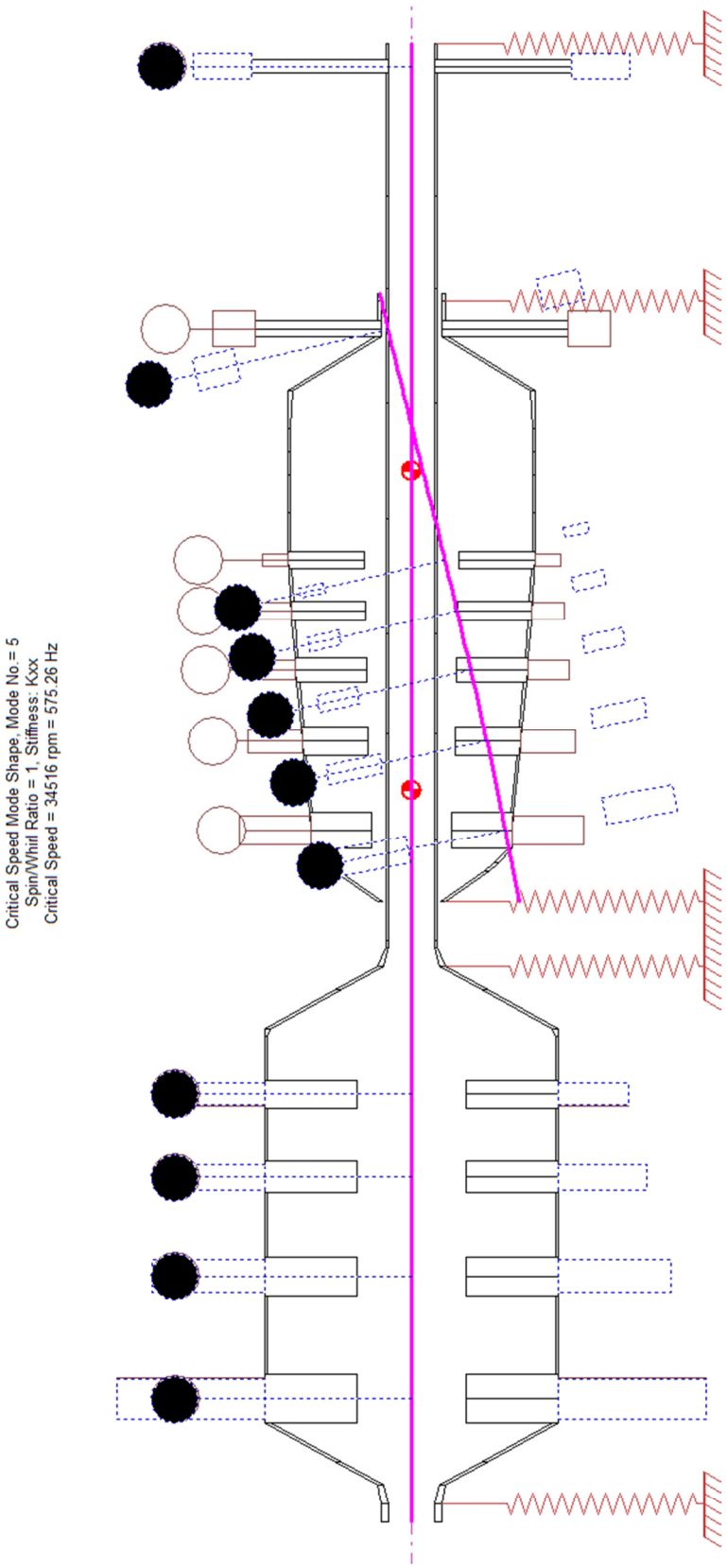

Appendix 10

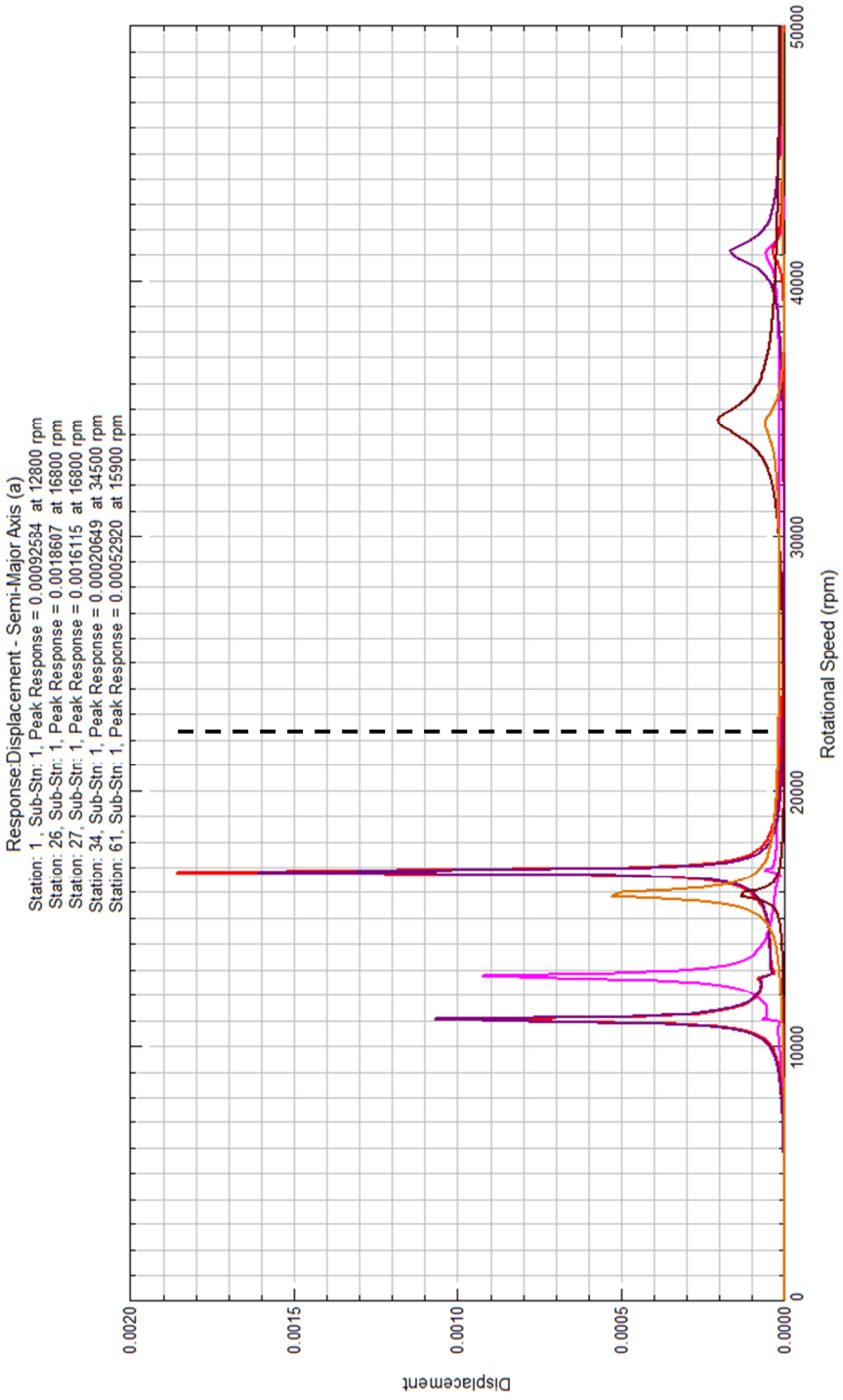
Response:Displacement - Semi-Major Axis (a)
Station: 1, Sub-Stn: 1, Peak Response = 0.00092584 at 12800 rpm
Station: 26, Sub-Stn: 1, Peak Response = 0.0018607 at 16800 rpm
Station: 27, Sub-Stn: 1, Peak Response = 0.0016115 at 16800 rpm
Station: 34, Sub-Stn: 1, Peak Response = 0.00020649 at 34500 rpm
Station: 61, Sub-Stn: 1, Peak Response = 0.00052920 at 15900 rpm
Displacement
0.0020
0.0015
0.0010
0.0005
0.0000
0
10000
20000
30000
40000
50000
Rotational Speed (rpm)